Progress in Quantum Electronics 85 (2022) 100394

Contents lists available at ScienceDirect

Progress in Quantum Electronics

journal homepage: www.elsevier.com/locate/pqe

Deterministic integration of single nanowire devices with on-chip photonics and electronics

D. Jevtics, B. Guilhabert, A. Hurtado, M.D. Dawson, M.J. Strain *

Institute of Photonics, Dept. of Physics University of Strathclyde Glasgow, UK

ARTICLE INFO

Keywords:
Integration
Nanowires
Semiconductors
Nanophotonics

ABSTRACT

The epitaxial growth of semiconductor materials in nanowire geometries is enabling a new class of compact, micron scale optoelectronic devices. The deterministic selection and integration of single nanowire devices, from large growth populations, is required with high spatial accuracy and yield to enable their integration with on-chip systems. In this review we highlight the main methods by which single nanowires can be transferred from their growth substrate to a target chip. We present a range of chip-scale devices enabled by single NW transfer, including optical sources, receivers and waveguide networks. We discuss the scalability of common integration methods and their compatibility with standard lithographic methods and electronic contacting.

1. Introduction

The design and growth of nanowire (NW) devices is reaching a significant level of maturity, enabling a myriad of devices with their associated advantageous optical and electronic properties [1–10]. Notable advances have enabled NWs with quantum well structures for electronic confinement and enhanced optical gain [5,11], nano-patterning [12] and vertically defined heterostructures for use as Bragg reflectors [13], NWs containing quantum dots for application as single photon emitters [14,15], and doped semiconductor materials for direct electrical injection [16]. The repeatability and yield of populations of NW devices on growth substrates is now sufficiently stable to allow the selection of individual devices for integration into chip-scale systems. This is an important step in the translation of NW technology from proof-of-concept demonstration devices to scalable system components.

The bulk transfer of large populations of NWs is a widely reported methodology allowing integration of sets of NW devices in a single shot [17] with no precise control necessary over individual device locations. These transferred populations of devices can be post-processed to form electronic devices for applications including flexible electronic contacts, junction devices [18] and sensors [19]. These bulk transfer methods are beyond the scope of this review. In this article we present a review of the fabrication techniques that have been developed for the deterministic integration of single NW devices in on-chip photonic and electronic applications. In Section 2, we present a number of complementary methods for the transfer of NW devices from their native growth substrate to a receiver substrate. A crucial element in the fabrication process is the integration of NW devices with on-chip system elements. This can be achieved using pre- or post-transfer integration of the NW's and examples of each methodology are given. These methods are compared in terms of the process complexity, throughput and positional accuracy. In Section 3 we present systems demonstrations enabled by the deterministic transfer of single NW devices. In particular NWs coupled to on-chip optical waveguides and electronic components are presented. Finally, in Section 4 we discuss recent advances being made to enable scaling of single NW technologies, including the high

* Corresponding author.
E-mail address: michael.strain@strath.ac.uk (M.J. Strain).

https://doi.org/10.1016/j.pquantelec.2022.100394

Available online 30 April 2022

speed characterisation of populations of devices, advanced growth methods for directed device transfer and high throughput printing methods.

2. NW transfer methods

In this section we review a range of methods for the integration of NW devices onto non-native substrates. We start with an introduction to the most common substrate transfer methods, where large populations of vertically grown NWs are mechanically cleaved and deposited on a secondary substrate. Although not providing deterministic transfer of single NWs themselves, these methods are often a precursor to high accuracy integration processes and are therefore an important stage in the fabrication flow. Following on from this we present a range of techniques for the integration of single NW devices on-chip, highlighting their spatial accuracy, yield and throughput. Finally, we present the major features of these methods in Table 1 to allow direct comparison.

2.1. Low spatial density mass transfer

The simplest approach by which NW devices can be transferred to a receiver substrate with low spatial density is via methods similar to mass transfer. The low spatial density on the receiver may be sufficient to enable addressing of single NWs either optically or electronically. Nevertheless, these methods are not examples of deterministic transfer and are typically used to fabricate devices making use of a number of nanowire devices simultaneously. Of these methods, the simplest is direct 'dry transfer' of NWs from their growth substrate to the receiver [20], where directional shearing forces can be used to coarsely align the long axes of NW devices. Fig. 1(a) shows a schematic of the dry transfer process. The vertically grown NWs on their native substrate are brought into direct mechanical contact with the receiver substrate. The samples are then translated relative to one another to promote shearing of the NWs and transfer to the receiver.

A modification of the simple direct transfer method is to use an intermediate, soft transfer substrate such as Polydimethylsiloxane (PDMS) [21]. In this case the PDMS is used to make contact with the donor substrate and the NWs are sheared and adhere to the PDMS. The PDMS is then brought into contact with the final receiver substrate and again a shearing relative contact is used to transfer the NWs. The yield of all direct transfer methods relies on the relative adhesion of the two surfaces, as well as the mechanical motion applied [21].

The initial cleaving of the NWs from their growth substrate can also be achieved using liquid assisted ultrasonic agitation [22]. In this technique the donor substrate is immersed in liquid and then subjected to vibration in an ultrasonic bath. The ultrasonic actuation induces cleaving in the NWs that are then suspended in the liquid. Submersion of a receiver substrate allows deposition of the NWs from suspension, or they can be allowed to settle on their native substrate and subsequently transferred by PDMS contact transfer.

The method by which the NWs are cleaved from their growth substrate has important implications for the facet quality, a crucial factor for NW laser devices. Cleavage is necessary not only in random low density transfer, but for all deterministic NW transfer techniques detailed below. Alanis et al. [22] show that the cleavage method, comparing direct mechanical contact, PDMS contact and ultrasonification, has measurable effects on the both the distribution of NW cleaved lengths and facet quality, as assessed through lasing threshold. Distributions of these variables in populations of transferred NWs are shown in Fig. 2(a) and (b). PDMS and short ultasonification are shown to produce transferred populations with the lowest spread of lengths and threshold energies. Examples of the facet

Table 1
Comparison of NW integration methods.

Integration Method	Throughput	Process Control	Spatial Accuracy	Rotational Accuracy	Receiver Substrate Requirements	Processing Environment
Direct transfer	Mass transfer	Manual/ Automated	Low control over individual devices	Limited, via shearing force	None	Table top
Ultrasonification + Direct Transfer	Mass transfer	Manual	Low control over individual devices	Limited, via shearing force	None	Ultrasonic bath + Table top
Direct Transfer + FIB Milling	Mass transfer/Single serial NW processing	Manual	Low accuracy device transfer/Sub-μm accuracy milling	Limited, via shearing force	Compatible with FIB milling process	FIB milling system chamber
Regrowth	Wafer scale integration via lithographic processing	Automated	Nanoscale accurate lithographic pattern definition	NA (vertically defined NWs)	Compatible with epitaxial growth processes	Semiconductor growth and processing
Micro-manipulation/ AFM probe transfer	Single device	Manual	Sub-μm accuracy	High accuracy	None	Table top/SEM chamber
Surface assisted Transfer	Single device	Manual	Sub-μm accuracy	High accuracy	Pre-fabricated surface topologies with sub-μm dimensions	Table top/SEM chamber
Optical trapping	Single device	Manual	Sub-μm accuracy	High accuracy	Compatible with liquid immersion	Liquid immersion + optical microscope
Transfer printing	Single device	Manual/ Automated	Sub-μm accuracy	High accuracy	None	Table top

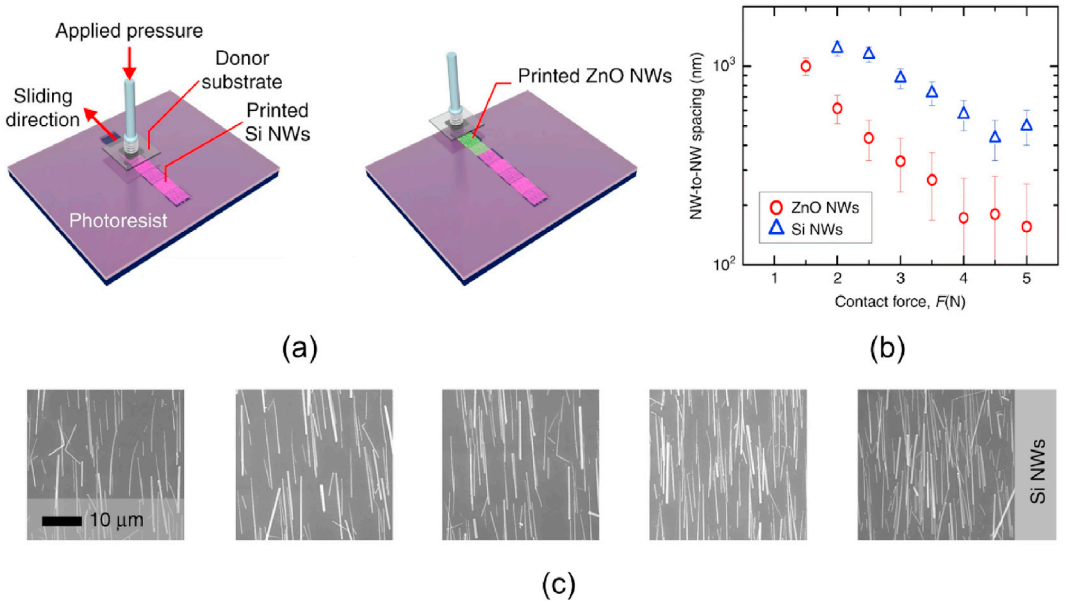

Fig. 1. (a) Schematic of a mass transfer of vertically grown NW devices to a receiver substrate by direct mechanical contact. (b) Measured NW-to-NW spacing as a function of applied transfer head force. (c) SEM images of silicon NWs with varying on-chip densities. Adapted under CC-BY license from Microsystems & Nanoengineering 4, 22 (2018). Copyright 2018 The Authors [20].

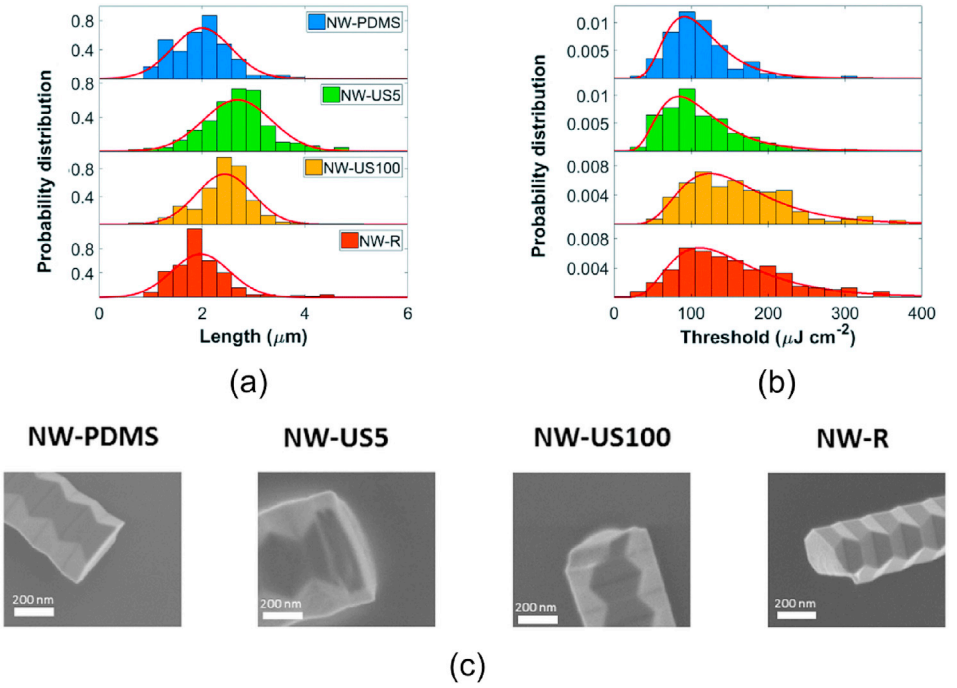

Fig. 2. (a) Measured NW length and (b) lasing threshold histograms for four methods of NW cleavage and transfer: 'R' direct transfer; 'US5′ 5s ultrasonification; 'US100′ 100s ultrasonification and 'PDMS' intermediate PDMS substrate transfer. (c) Example SEM images of cleaved NW device facets. Republished with permission of Royal Society of Chemistry, from Ref. [22].

damage induced by each of the four cleave and transfer methods are shown in Fig. 2(c). The PDMS transfer and short ultrasonification, corresponding to their lower threshold values, can be seen to exhibit more uniform facet cleave planes.

2.2. Self-aligned NW devices

For systems where NWs can be integrated with other components through post-transfer fabrication methods, or by simple free space optical pumping, random distributions on chip may be sufficient. However, in systems where alignment of NWs with other NWs or sub-micron chip features are required, then higher spatial accuracy methods are necessary. One such method makes use of NW structures as a basic unit to be sub-divided [23]. Gao et al. show that NW devices can be sub-divided into optical sub-cavities using a targeted Focused Ion Beam (FIB) milling to etch a trench across the device. The technique uses a metal mask deposited on the NW during the milling to protect the device from deposition of Ga ions that would alter its electronic and optical properties. The mask is removed post-milling via a wet chemical etch. This method preserves alignment between the two sub-cavities and allows for extremely compact gaps between their facets in the order of 100 nm, minimising diffractive losses between cavities. Dual cavity NW laser devices fabricated in this manner, with the FIB milled gap as a parameter, exhibit control over the longitudinal lasing modes. Although a very spatially accurate method, this technique requires serial processing of devices and is limited to structures that can be fabricated using a single original NW.

2.3. Regrowth of III-V NWs on silicon

Although not strictly a transfer method, it is worth highlighting the epitaxial growth of semiconductor NW devices directly on silicon photonic circuits. Kim et al. [4,24] demonstrate the growth of semiconductor NW emitters on silicon-on-insulator substrates pre-patterned with silicon waveguide structures. By using a site-specific growth method, the authors demonstrate accurate definition of vertically grown NWs in a periodic array on the silicon waveguide mesa. This periodic array enables efficient coupling from the optically active III-V NWs to the planar silicon waveguide structures.

2.4. Micro-manipulation with needle tips and AFM probes

A significant advance in NW integration technologies has been the use of micro- and nano-manipulators for the deterministic transfer of single devices. Typically, populations of NWs are transferred to an intermediate substrate using direct mass transfer to cleave devices from their native substrate and then individually selected and transferred to the receiver substrate. Simple variations of this technique can be realised using an optical microscope, translation stage and a needle probe tip [25–29]. Although limited in spatial accuracy these probe manipulation methods are extremely flexible and allow the user to pick-up individual NWs or ‘nudge’ them into position on a surface. The alignment of individual NWs to on-chip structures can reach the sub-micron accuracy level, but is strongly dependent on

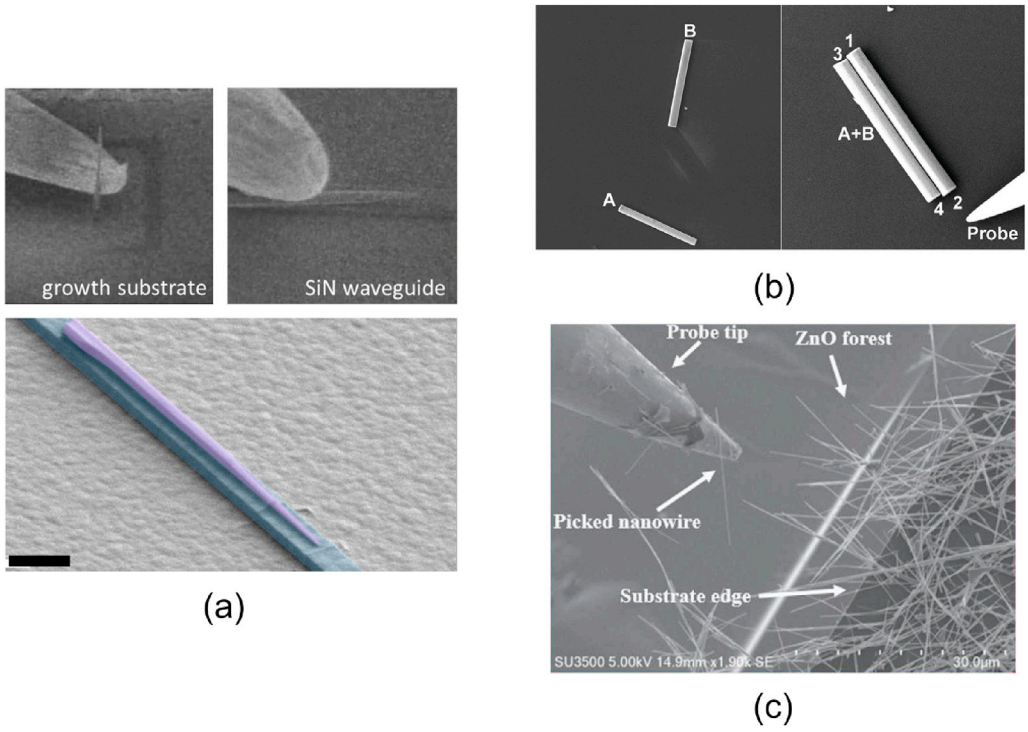

Fig. 3. Examples of single NW devices transferred in-situ in SEM systems: (a) Micro-tip pick-up and deposition of a semiconductor tapered NW on a SiN waveguide. Reprinted from Ref. [14]. Copyright 2020 John Wiley & Sons, Inc. (b) Manipulation of a pair of GaN NW lasers into a coupled cavity geometry. Reprinted from Ref. [36], with the permission of AIP Publishing. (c) SEM image of a nanomanipulator probe tip with NWs adhering to the surface from failed transfers. Copyright 2021 IEEE. Reprinted, with permission, from Ref. [35].

manual control of the system and typically requires substantial time to overcome yield issues. Furthermore, the adhesion of NW's to probe tips with micron scale radii of curvature is not easy to control, dependent on relative geometry of the probe and NW, probe and target substrate materials and mechanical transfer techniques such as shearing or rotation of the probe that can reduce spatial accuracy. Contamination of the probe tip is common with NWs that have not transferred or have been picked up unintentionally, as shown in Fig. 3. The selective deposition of NWs from the micro-probe tip can be improved by employing a second probe to operate in parallel, improving yield of transfer and spatial alignment to receiver substrate structures [30,31].

An improvement of the micro-manipulation method makes use of high resolution in-situ imaging to guide transfer, for example with Atomic Force Microscopy (AFM) [32,33], or Scanning Electron Microscopy (SEM) tools [14,34–36]. The high magnification imaging of the NW devices and target substrate structures, along with accurate nano-manipulator probes, allows manual control and alignment of NW devices, though with limited throughput. Fig. 3 shows examples of single NW devices aligned to receiver substrate structures with accuracy substantially below 1 μm.

These in-situ, high magnification image solutions provide excellent spatial transfer accuracy for single NW devices, but remain limited in terms of throughput due to the manual nature of the process and the probe tip adhesion limited yield.

2.5. Assisted NW transfer

Two main methods have been developed to address the challenge of yield in micro-probe based transfer. In the first, topological features in the receiver substrate are used to mechanically promote detachment of the NW from the probe. In the second, an electric field is generated aligned with the target position on the receiver substrate to direct adsorption of NW devices held in a liquid suspension.

An excellent example of the first method combines a topological trapping feature with a functional optical element on the receiver chip. Bermundez-Urena et al. use a V-groove in a metal surface as a plasmonic waveguide that can couple to the emission of a deposited NW laser device [37]. Fig. 4 shows a schematic and SEM image of the NW laser deposited in the V-groove plasmonic waveguide. The V-groove structure performs two optical functions. Firstly, it is designed to efficiently couple light between the lasing mode of the NW cavity and the surface plasmon mode of metal surface, and secondly, the angled ends of the groove couple the guided light into free space for measurement.

In this approach a single NW is picked up from an intermediate surface using a micro-probe and is brought into contact with the receiver surface. The micro-probe is then used to translate the NW across the surface to the position of the V-groove, where the local topology provides a favourable condition for the NW to be deposited in the groove, rather than follow the probe translation. Not only does this method increase the likelihood of NW transfer from the micro-probe to the surface, the geometry of the V-groove allows for self-alignment of the NW with the plasmonic waveguide axis, without the necessity for high accuracy micro-probe rotational control. This method has also been employed in SiN based photonic crystal waveguide designs, where a central grove is incorporated to aid

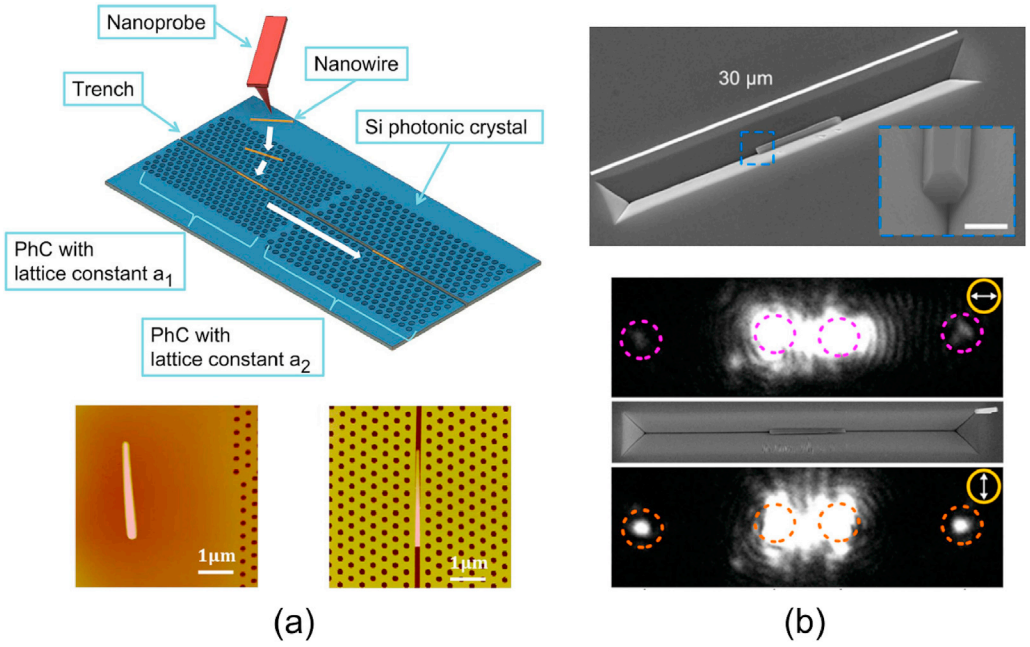

Fig. 4. (a) Schematic and AFM images of a NW manipulated into a topological groove in a silicon photonic crystal device. Adapted with permission from Ref. [32]. Copyright 2017 American Chemical Society. (b) SEM image of a plasmonic V-groove waveguide with an integrated NW laser. Lower images show vertically scattered optical emission from the NW under variable polarisation pumping. Efficient coupling to the plasmonic V-groove mode and out-coupling facets is shown in the bottom image. Adapted with permission from Nano Letters 17, 6b03879 [37]. Copyright 2017 American Chemical Society.

transfer of sub-100 nm diameter NWs [32,38].

To enable electric field assisted transfer, NWs must be first cleaved from their growth substrate and incorporated into a liquid suspension. The density of deposited devices on the target substrate can be controlled through the volume density of NWs in the original suspension. Smith et al. [39] present an electric field assisted deposition method using inter-digitated contact tracks on the receiver substrate. A bias applied across these tracks induces a polarisation field in the NWs in suspension, aligning them with the field generated on the substrate and promoting localised deposition of the conductive NWs. Density of deposited NWs can be controlled through local field intensity control and applied voltage. Fig. 5 shows two variations of the process, with the contacts in Fig. 5(b) optimised to produced single NW device deposition.

2.6. Optical trapping

Optical trapping of micro-particles is a well established technique, utilising structured illumination fields to create displacement force gradients in particles in suspension [40]. These structured light fields can be controlled to trap and manipulate particles in real-time and with good spatial accuracy [41]. This method has been applied to NW devices and by making use of scanning lasers [42] and spatial light modulator (SLM) technology, not only can devices be positioned on a substrate, control be exerted over multiple NWs simultaneously and devices can be manipulated in translational and rotational motion, as shown in Fig. 6. Furthermore, by combining optical trapping with laser processing, Agarwal et al. [13] show that single NWs can be trapped and cleaved into smaller sections, or multiple devices can be laser fused into proto-circuit arrangements, as shown in Fig. 6. As with the micro-probe manipulation methods, optical trapping is low throughput and requires significant manual control to select suitable devices from suspension volumes, though the control it affords is significant.

2.7. Transfer printing

Of all the micro-manipulation methods, transfer printing is the most compatible with automation and high device throughput. As is the case with micro-probe transfer, this technique requires an initial stage of mechanical transfer of vertically grown NWs from their growth substrate to an intermediate receiver, where the NWs are randomly arranged, horizontally on the surface. Individual NWs can then be selected and transferred to a final receiver substrate individually. Transfer printing instruments are typically based on an optical microscopy system and a high resolution translation stage, on which the donor and receiver samples are mounted. The basic principle of operation is similar to the micro-probe methods detailed above, but can be carried out without the need for in-situ SEM imaging and manual control of micro-probe tips. The transfer method uses micro-fabricated PDMS stamps that allow for spatial addressing of single NWs. Details of the basic printing system and methodology are given in Ref. [43].

2.7.1. Methodology

Transfer printing was developed initially as a method for the spatially controlled transfer of thin film semiconductor and organic membranes [21]. As in some other forms of mass transfer, an elastomeric polymer stamp, usually of PDMS, is used to transfer thin films from one substrate to another. A key advance in transfer printing methods is that the PDMS stamp can be microfabricated to present topological features that allow for the individual addressing of single, isolated devices on-chip. PDMS stamps can be fabricated using standard lithographic methods, enabling single print heads or arrays of pick-up heads, fabricated to match the layout of membrane devices being transferred. This technique allows for the selection and transfer of small area membranes, with thicknesses from a few hundred nanometres to a few micrometres, and cross sectional areas in the range of $5 \times 5\ \mu m^2$ to $1 \times 1\ mm^2$. To enable this selective area transfer, both the donor substrate and stamp material can be processed with micron scale features. A schematic of a basic transfer

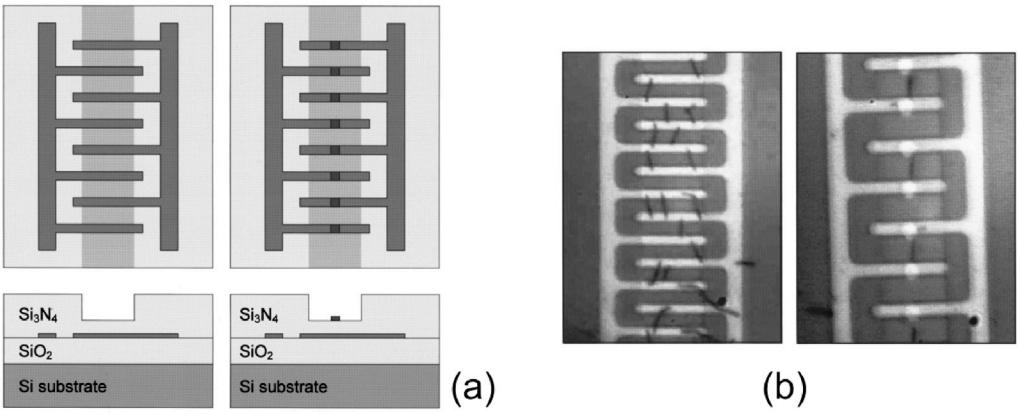

Fig. 5. (a) Schematic of inter-digitated contact arrangements for conductive NW alignment and transfer. (b) Optical microscope images of 5 μm long Au NWs on inter-digitated electrodes. Multiple NW devices (left) and single NW devices (right) aligned to the contact electrodes. Reproduced from Ref. [39], with the permission of AIP Publishing.

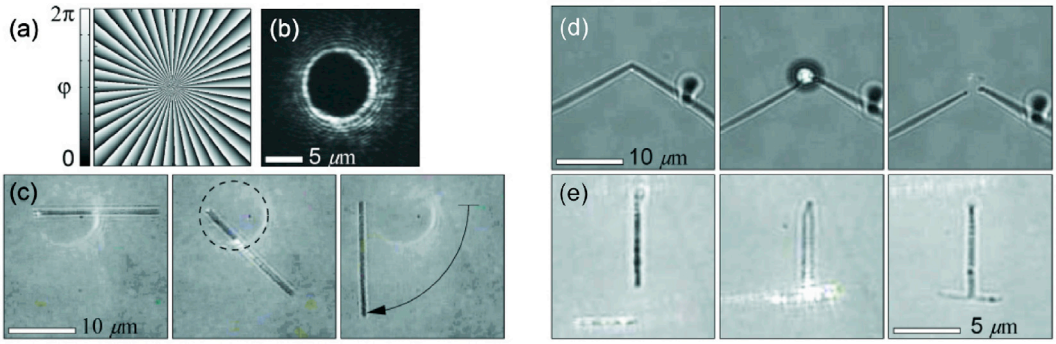

Fig. 6. Optical trapping and manipulation of NWs. (a) SLM phase mask used to generate an Orbital Angular Momentum (OAM) carrying beam (b). (c) Microscope images of a NW held in the OAM beam trap. The orbital angular momentum density in this trap can be used to rotate a semiconductor nanowire, as shown in the sequence of photographs which are separated by 1 s intervals. (d) and (e) show the cleaving and fusing of NW devices using optical fields respectively. Adapted from Optics Express 13, 22 (2005) [13]. Copyright 2005 Optical Society of America.

printing process is shown in Fig. 7(a). The process makes use of a differential adhesion effect between the PDMS stamp and the membrane to be transferred. First, the PDMS stamp is fabricated to present a micro-pillar that is similar in cross-sectional area to the membrane devices to be transferred. The stamp can then be mounted in the transfer print instrument, suspended rigidly between the microscope head and the translation stage where the substrates are mounted. PDMS is transparent at visible wavelengths, allowing for imaging through the stamp material during the processing. On the donor substrate, the membranes are often prepared for printing using a selective under-etch process [44–46]. This allows suspension of thin membranes over their native substrate, supported by micron scale tethers that are cleaved during the printing process. The adhesion of the PDMS stamp to the membrane is dependent on the contact area between the two and the velocity with which the stamp is retracted relative to the substrate, see Fig. 7(b) [21]. Therefore, a fast retraction can be used to overcome bonding forces of a membrane on its native substrate, either through contact or tether supports, and a slow retraction allows deposition of the membrane onto the target substrate.

There are two factors in this methodology that require attention when considering the transfer of NWs rather than flat membrane devices. Firstly, NWs are typically only a few microns in length with a cross-sectional diameter in the tens to hundreds of nanometres range, and therefore it is extremely difficult to fabricate transfer stamp features matching in size. Secondly, NWs are typically in full contact with an intermediate substrate after cleaving from their growth substrate, and so cannot make use of the lithographically defined spatial registration or suspended geometries of thin film planar membranes.

Micro-stamps for NW transfer have been fabricated with cross-sectional dimensions in the few microns range [47]. Although much larger than the NW devices themselves, single NWs can be selected through the surface density coverage of devices, allowing only a

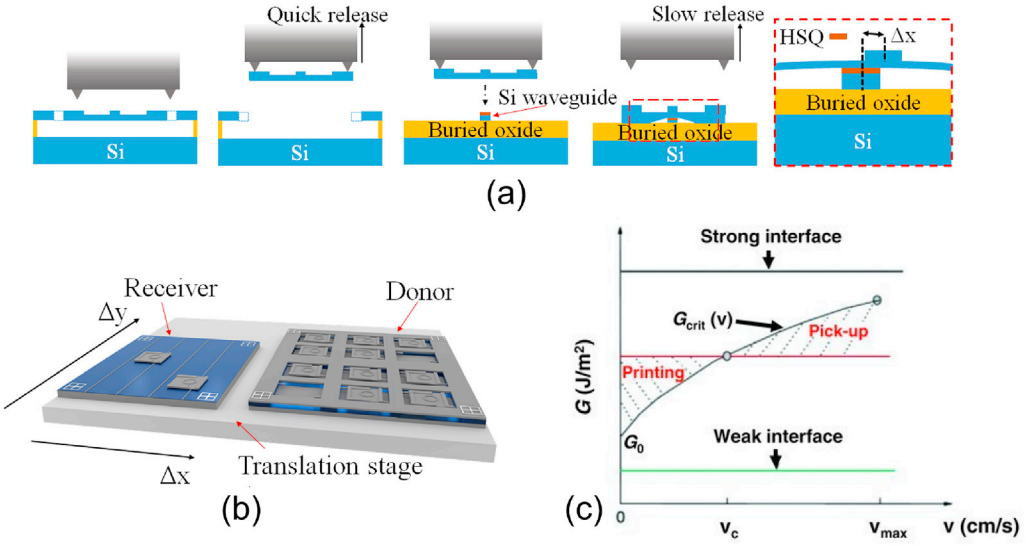

Fig. 7. (a) Schematic of a membrane transfer printing process for a silicon photonic membrane onto an silicon-on-insulator waveguide. (b) Schematic view of donor and receiver substrates. Adapted under CC-BY 4.0 license from Optics Express 26, 13 (2018). Copyright 2018 The Authors [46]. (c) Critical energy release rates for PDMS stamp based membrane printing. Low release velocities correspond to printing to a surface and higher than critical energy G_{crit} rates demonstrate membrane pick-up. Republished with permission of John Wiley & Sons - Books, from Ref. [21].

single device to be addressed by the stamp. The full surface contact of the stamp is further enhanced by PDMS deformation around the NW, allowing detachment of the device from its donor substrate. A schematic and optical micrographs of a NW printing process following this approach are presented in Fig. 8. The curing conditions of the PDMS stamp may also be used to control its adhesive force that, together with selection of an intermediate donor substrate, can be used to improve pick-up and transfer yield. Further discussion on PDMS adhesion control is presented below with respect to dense device integration. Additionally, as with the micro-probe based methods, topological structure on the receiver substrate can be used to improve transfer yield, for example through shearing force detachment of the NW from the PDMS stamp.

2.7.2. Spatial accuracy

The major challenge for transferring NW devices with high spatial accuracy is that they are typically randomly distributed on the donor substrate, unlike membrane devices which are defined lithographically and can therefore be related to optimised marker structures. Integration of NW devices with on-chip photonic or electronic components requires spatial accuracy in the sub-micron range, including control over the angular direction of the NW long axis.

Topological features can be used to ensure NW alignment with on-chip structure, particularly if these features correspond with the optical or electronic devices being targeted, for example in the case of V-groove waveguides [28,37]. Alternatively, the large aspect ratio between the NW diameter and long axis length can be used effectively to self-reference the NW position and orientation using simple optical microscopy techniques. McPhillimy et al. show a method by which NWs can be spatially referenced on their donor substrate using an image correlation method between the image of the NW and a template line object held in computer memory. Translations in the xy-plane, along with rotations of the template image, allow precise location of the NW and orientation information to be measured relative to the coordinate system of the translation stage in the printing instrument. The same spatial registration process can be carried out on the receiver substrate, providing a translation and rotation function between the NW donor and receiver positions. Fig. 9 shows NW devices that have been printed next to lithographically defined silicon gratings, or already positioned NWs, using this method. Fig. 9 also shows scatter plots of the translational and rotational accuracy of the NW transfer method from Ref. [48], highlighting the excellent control afforded by this technique.

2.7.3. Serial printing and dense integration

One of the key benefits of NW devices is their compact footprint, allowing for dense integration of components on-chip. The large cross-sectional area of the transfer print stamp compared with the NW poses a challenge to the serial integration of devices in close proximity. In particular, the footprint of the PDMS stamp is such that it will come into contact with an already deposited NW when printing the next device in the series. As noted above, the risk of re-pick up of the first NW can be significantly reduced by careful design of the process and adhesiveness of the target substrate and stamp. In Ref. [47] Jevtics et al. demonstrate a method by which multiple NWs from different growth platforms can be printed in areas similar to the NW footprint. An intermediate substrate stage is used to allow high-yield pick up from the donor and then high yield deposition to the receiver. A schematic of the process is shown in Fig. 10.

In Ref. [47] there is a characterisation stage in the transfer process that is used to select individual devices for integration on the final chip. This stage is not fundamental to the serial printing process. The crucial element of this method is that the final PDMS stamp used to contact the receiver substrate is below the threshold to pick-up the in-situ NW when retracted during the process step for the next NW in the serial printing process. Using a silica receiver substrate, this is found to be possible for a PDMS stamp fabricated using an 8:1 ratio of

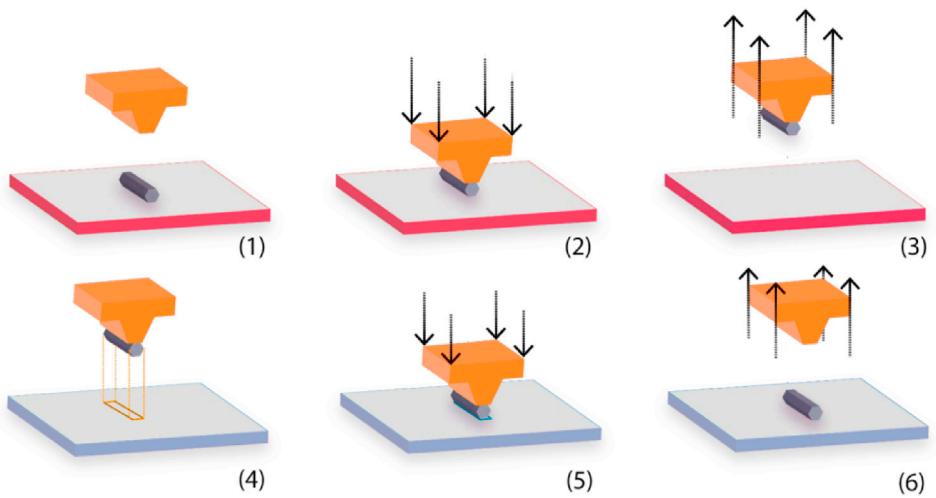

Fig. 8. Schematic of a NW transfer printing process. (a) The transfer stamp head is aligned to the NW on its donor substrate, (b) the PDMS stamp head is brought into contact with the NW, (c) the NW is released from the substrate at a velocity above the critical point, (d) the NW device is aligned to its receiver substrate position and (e) brought into contact with the surface, (f) the PDMS stamp head is removed at a velocity below the critical point leaving the NW deposited on the receiver substrate.

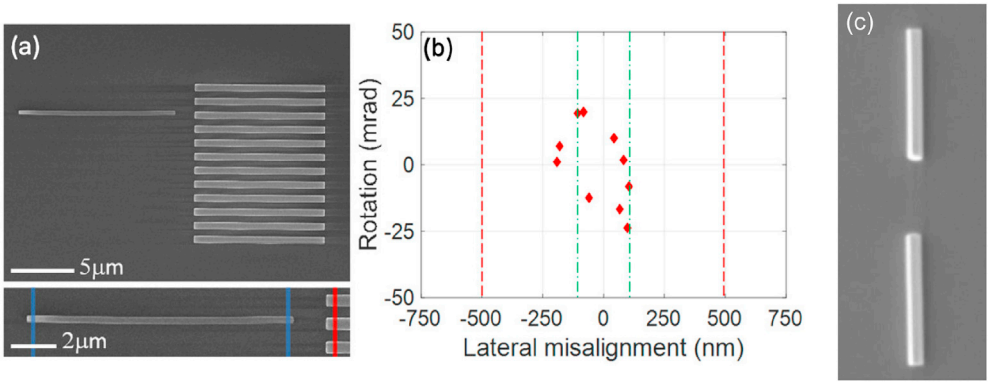

Fig. 9. (a) SEM images of an InP NW, aligned with a silicon grating with 500 nm mark/space features. (b) Lateral and rotational alignment achieved using automated NW alignment process and print. Adapted with permission from ACS Applied Nano Materials 3, 0c02224 [48]. Copyright 2020 American Chemical Society. (c) Two 5 μm long NWs printed with their axes aligned. Adapted with permission from Ref. [49]. Copyright 2017 American Chemical Society.

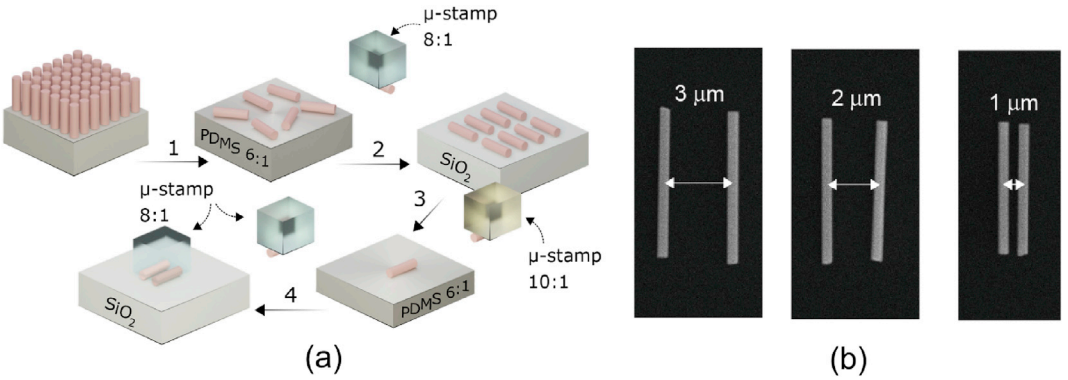

Fig. 10. (a) Schematic of the dense integration NW printing, making use of intermediate substrates and different PDMS stamp heads to enable deterministic single device transfer. (b) SEM images of fabricated devices with inter-device spacing down to 1 μm. Adapted under CC-BY 4.0 license from Optical Material Express 11, 10 (2021). Copyright 2021 The Authors [47].

PDMS to curing agent. Fig. 10 shows SEM images of NWs that have been printed side-by-side within a few micrometres of one another in such a serial process.

2.8. Comparison of integration methods

Table 1 presents a comparison of the integration methods presented above, with parameters including spatial and rotational accuracy, throughput, automation and processing requirements.

3. Integration of NWs with on-chip structures

The above detailed integration processes have been used to demonstrate integration of NW devices for a range of applications, including enhanced optical emission, electronically addressed optical receivers and mechanical sensing components. A few such demonstrator systems are detailed below as examples.

3.1. On-chip grating devices

NW devices are attractive due to their very compact footprint, but this in turn makes it more challenging to integrate these devices with traditional opto-electronic elements. Bragg gratings are a widely employed optical device in integrated photonics for wavelength selective filtering, controlled optical feedback or vertical emission for off-chip coupling. NWs can be connected with these type of structures through intermediate coupling to waveguide elements, as discussed below, or through direct integration onto grating elements.

Xu et al. [50] demonstrate NW devices integrated with circular, vertical emission grating elements, fabricated both by FIB milling of

gratings post-NW deposition and printing of NWs directly onto pre-fabricated gratings. An example of a post-transfer fabricated circular metallic grating integrated with a semiconductor NW laser is shown in Fig. 11(a). The grating elements couple the optical modes of the NW lasers to vertical emission modes, additionally providing cavity selection effects for polarisation and directionality of the vertically coupled modes.

NW lasers have also been directly transferred onto in-plane Bragg grating elements for lasing mode selection. Wright et al. demonstrate integration of GaN based NW laser devices with SiN on-chip Bragg gratings [51], as shown in Fig. 11(b). The refractive index contrast of the on-chip Bragg grating is in direct contact with the NW surface, providing an index perturbation to the evanescent tail of the guided lasing modes of the NW. This distributed Bragg reflector is shown to provide feedback selection amongst the guided modes of the NW, with wavelength discrimination using the relative rotation of the grating and NW axes, i.e. changing the effective grating period apparent to the NW modes.

3.1.1. Optical receivers

NW devices, with their strong optical and electronic confinement, are attractive components for compact on-chip detectors, and can be directly addressed with electronic contacts. Yang et al. [52] present spectrally resolved photo-detection in the visible range of the electromagnetic spectrum, using only a single NW detector. By grading the material composition of the NW during growth, with constituent components of Cd, S, and Se, the authors show that the local bandgap of the NW can be spatially controlled. A single NW is deposited on a silica substrate and post-fabricated with micron scale In/Au contacts along its length, as shown in Fig. 12(a). The spectrally resolved absorption of incident light can then be extracted from the photo-current measured across the array of contacts to the NW. Although still limited in spectral resolution, this ultra-compact device is competitive with devices with significantly larger footprints.

The compact geometry and high intrinsic field gradients in NW devices, make them attractive for single photon sensitive detection at room temperature [53,54]. In Ref. [53] the authors demonstrate integration of a single core-shell NW detector with electronic contacts for single photon detection, see Fig. 12(b). The core-shell electronic confinement enables photon number resolving detection at room-temperature. Furthermore, the nanowire geometry produces polarisation anisotropy in detection efficiency, paving the way for future room temperature arrays of polarisation sensitive photon counting detectors.

The electronic confinement and geometry of NW devices also make them suitable for polarisation sensitive detectors in the THz range of the electromagnetic spectrum. Peng et al. present polarisation selective THz detectors based on pairs of NWs with orthogonally

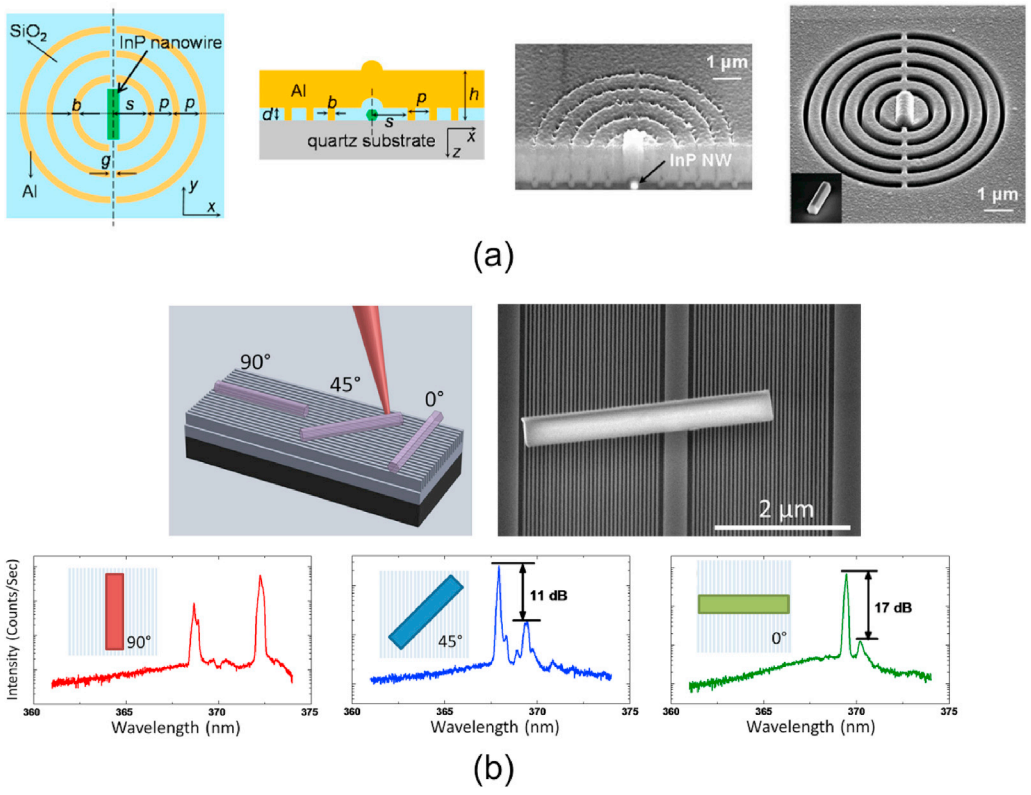

Fig. 11. (a) Schematic and SEM images of NWs integrated with metallic surface gratings for vertical emission enhancement. Adapted with permission from Ref. [50]. Copyright 2018 American Chemical Society. (b) NW laser integration with surface relief distributed Bragg reflectors for lasing mode selection. Reproduced from Ref. [51], with the permission of AIP Publishing.

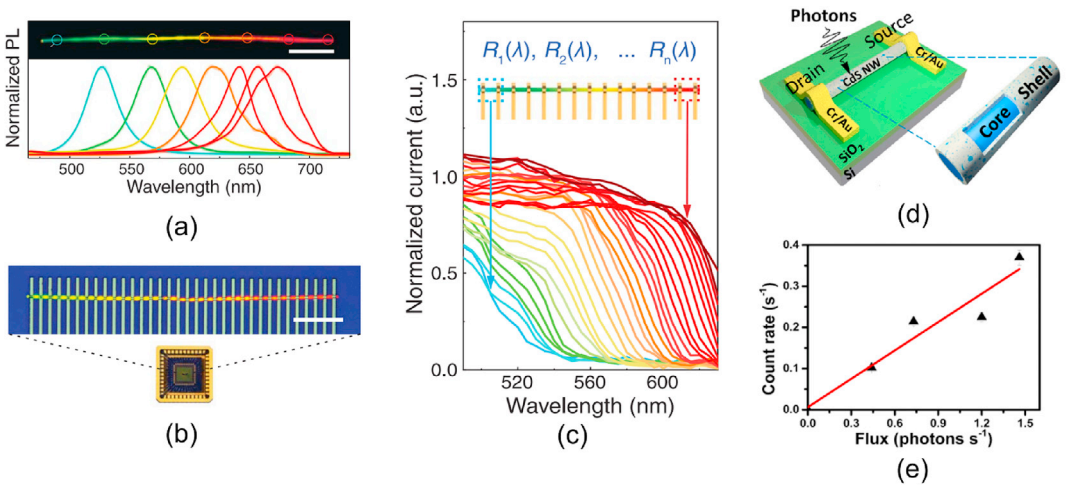

Fig. 12. (a) Photoluminescence measured from a graded composition Cd(S,Se) NW with spectra corresponding to indicated areas on the NW. (b) Microscope image of the electrically segmented and contacted NW spectrometer and the electronic package. (c) Photo-current response from each NW segment as a function of illumination wavelength. Republished with permission of American Association for the Advancement of Science, from Ref. [52]. (d) Schematic of a CdS core-shell single photon detector. (e) Measured count rate as a function of incident photon flux. Adapted with permission from Ref. [53]. Copyright 2018 American Chemical Society.

arranged axes [55]. These devices integrated two pairs of NWs with electronically contacted bow-tie antennas. The NWs were integrated with the electrical contacts in two stages, allowing the perpendicularly arranged NWs to be arranged in a vertical stack, thus addressing a compact area for polarisation resolved measurements. Fig. 13(a) and (b) show a schematic and SEM image of the crossed NW receivers. Fig. 13(c) presents the polarisation resolved measurements of the crossed NW detector system.

3.2. *Electrically addressed NW devices*

Electronic contacting of devices is a fundamental requirement for many on-chip systems and has been the focus of efforts in NW integration, in particular for the creation electrically pumped NW optical emitters [56,57]. Typically NW devices are transferred to their host substrate and electronic contacts then formed using lithographic mask and metal deposition methods, see Fig. 14(a).

Electronically pumped NW laser devices are a key component in many of the applications being targeted and a recent review [56] provides a broad overview of efforts being made in the area. An electrically pumped NW optical emitter device was demonstrated in 2003 by Duan et al. [58]. In this work a single CdS NW was transferred onto a p-doped silicon substrate and subsequently clad with an

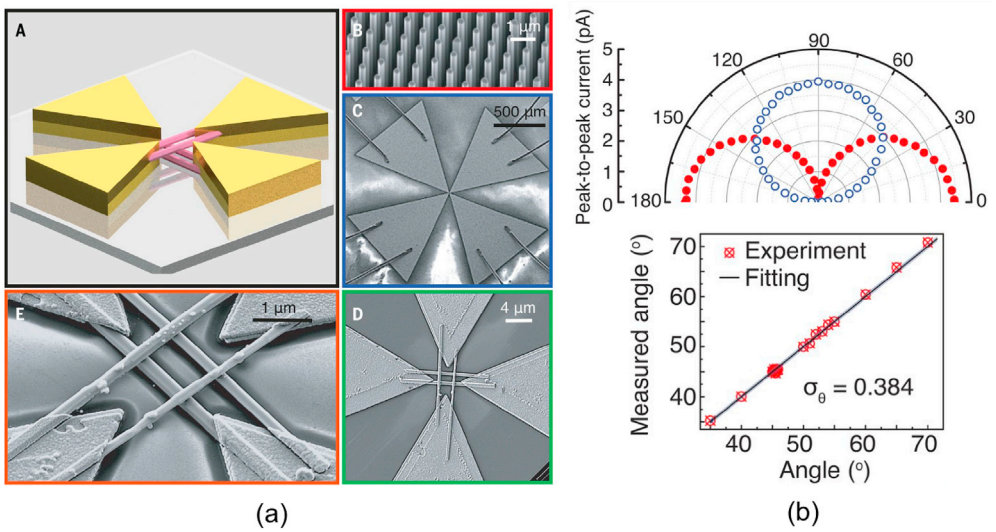

Fig. 13. (a) Schematic view and SEM images of the crossed NW THz detector and the donor NW array. (b) Polarisation dependent measured photocurrent in the horizontal channel (red dots) and vertical channel (blue circles) and (bottom) Extracted field angle from the two channel measurement. Republished with permission of American Association for the Advancement of Science, from Ref. [55].

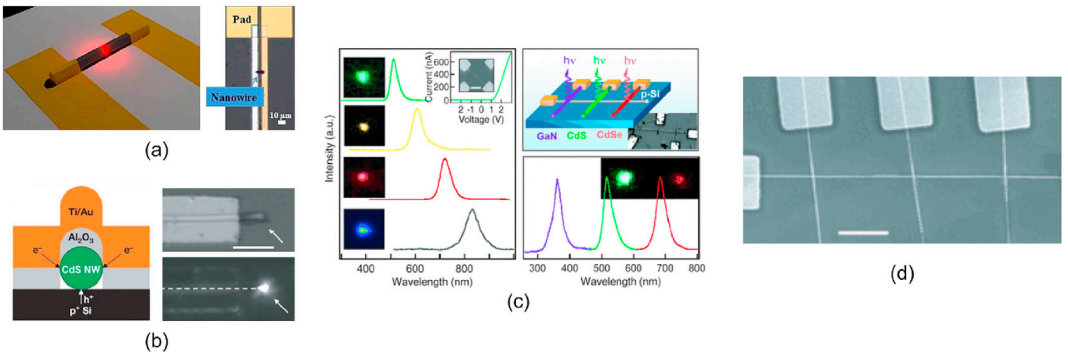

Fig. 14. (a) Schematic and optical microscope images of an electrically contacted NW LED device for direct modulation. Reprinted from Ref. [57], with the permission of AIP Publishing. (b) Schematic and microscope images of an electrically pumped CdS NW laser. Republished with permission of Springer Nature BV, from Ref. [58]. (c) Emission spectra from NW LED devices directly contacted using a doped silicon NW bus contact and (d) SEM image of the device. Republished with permission of John Wiley & Sons - Books, from Ref. [16].

Al_2O_3 layer for electronic insulation. Pinch points at the device edges allowed electronic injection from a metal contact layer deposited on the alumina cladding, as shown in Fig. 14(b). There is a clear trade-off in electrically pumped NW devices between the physical geometries required to inject carriers, via doped substrates or metal coatings, and the associated intra-cavity losses these induce. Advances in the state-of-the-art require multiple crucial challenges to be addressed, including optimised doping of NWs for electronic transport and the formation of metal contacts to minimise optical cavity losses.

Huang et al. [16] present an alternative mesh based technique for the compact integration and addressing of NW emitters with a

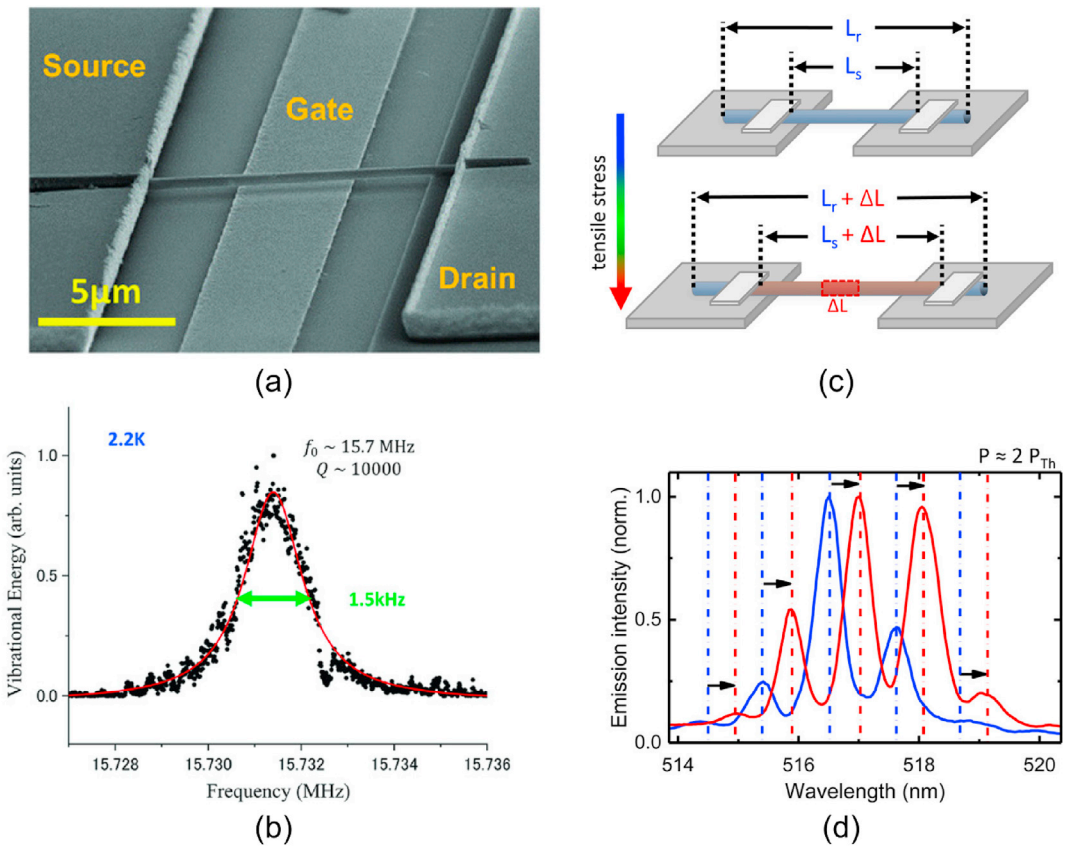

Fig. 15. (a) SEM image of a suspended NW acting as an RF coupled Nanomechanical Resonator and (b) low temperature mechanical resonance spectrum. Republished with permission of John Wiley & Sons - Books, from Ref. [59]. (c) Schematic of a NW emitter mounted between two silica supports. Uniaxial stress was applied through 3-point bending load applied to the substrate. Adapted with permission from Nano Letters 17, 7b02589 [60]. Copyright 2017 American Chemical Society.

range of optical emission wavelengths from the UV to the near-IR. A p-type silicon NW is used as a common conductor and terminated using a metal contact pad, as shown in Fig. 14(c). Individual semiconductors of a variety of material compositions make contact with the p-type silicon wire with their long axes perpendicular to that of the silicon wire. Each individual semiconductor NW is terminated at a contact pad. In this way each emitter can be electronically addressed and operated as a compact LED device.

3.3. Nanomechanical resonators

In addition to the applications in electronic and photonic systems that have driven NW research in recent years, individual, suspended NWs are an attractive option for Nano-Electro-Mechanical Systems (NEMS). In Ref. [59] Tomita et al. present the integration of a single InAs NW with metallic contacts, suspended over a gate electrode, using liquid assisted micro-probe transfer. An SEM image of the device is presented in Fig. 15(a). The mechanical vibration properties of the NW beam were measured using an RF mixing technique, showing resonances in the MHz range and voltage control of the device properties. The use of NW devices in this application allows decoupling of the fabrication process of the NWs from the surrounding electronic circuit elements, giving much greater flexibility to the mechanical geometries available. Furthermore, use of heterogeneously integrated NWs provides access to a variety of materials that could be used in a single compact system.

In Ref. [60], the authors integrate a NW device in a suspended geometry between two silica pads. By stressing the chip substrate in a three-point load bending setup, the NW can be put into tensile stress and the effective Fabry-Perot cavity length modulated. Direct measurement of the cavity spectrum shows modulation of the resonant cavity modes as an effect of the mechanical deformation of the NW, as shown in Fig. 15(d).

3.4. Integration of NWs with on-chip waveguides

As noted in the fabrication section above, high spatial accuracy of NW devices with on-chip waveguide devices is required to ensure efficient optical coupling between them. This alignment can either be achieved by post-transfer position registration of the NWs and subsequent fabrication of aligned waveguides, or by accurate transfer of NWs to already fabricated waveguide devices. Alternatively, sufficiently long NW devices can be used as waveguides themselves, and can be manipulated into coarse waveguide networks using the methods described previously.

3.4.1. NW based waveguides

The high refractive index contrast of semiconductor NWs to air, or a low refractive index substrate such as silica or polymeric materials, allows for strong optical confinement in NWs with diameters as low as a few hundred nanometres. Sirbuly et al. [38] show how simple mechanical contact of NWs can allow evanescent field coupling between devices and simple networks of waveguides can be formed, see Fig. 16. Light is shown to propagate along millimetre lengths of NW waveguide and measureable coupling is demonstrated amongst NWs of different material structures. NWs integrated with plasmonic waveguides can also be achieved using direct proximity coupling, as detailed in Ref. [29].

By manipulating long NW devices, multiple sections of a single device can be brought into close proximity, or contact, to form resonant cavity structures. Li et al. [61] show NW devices that are formed into compact resonator structures, including a cross-ring waveguide component, as shown in Fig. 16. The main lasing cavity in these structures is the Fabry-Perot cavity between the facets of the NW. In addition, the evanescent field coupling between the NW sub-sections allows for sub-cavities to be formed, and modal selection using a multiple cavity resonance effect. Such resonant cavities can also be embedded in elastomeric materials, so that on deformation of the host substrate, the geometric cavity is modified and an associated wavelength shift of the lasing mode can be measured, as detailed in Ref. [62].

3.4.2. Post NW transfer waveguide fabrication

Since waveguide devices can be fabricated post-transfer of NWs, this method of integration is compatible with randomly distributed devices, with the spatial accuracy provided in the lithographic stage of the process. Tchernycheva et al. [63] present integration of an InGaN NW LED, a silicon nitride waveguide channel and an InGaN NW photodetector in a single optical transmission channel demonstration. The NW LEDs and photodetectors were deposited separately on the host substrate with low spatial control. The positions of these devices were registered and used as references in the fabrication of a SiN waveguide channel. The SiN waveguide was fabricated using PECVD deposition and electron-beam lithography, ensuring good alignment with the NW devices and subsequently, the deposited metal contact tracks. Fig. 17(a) shows an optical micrograph of the fabricated system.

Better control over NW placement on the receiver substrate is important for future scaling of this form of integration. Post-alignment of waveguides to randomly placed NWs is resource intensive and requires new lithography patterns for every device instance. Furthermore, the position of NWs can frustrate efficient use of chip space or future integration with other components. Elshaari et al. present a refinement of the above method for fabrication of quantum dot containing NWs as a photon source for on-chip quantum photonic applications [27]. In this work the authors make use of on-chip markers to direct the micro-probe transfer of the NW emitters to desired locations on chip. The NWs in use are tapered to promote optical coupling between the wire and waveguide devices, as shown in a previous work where the NWs were embedded in SiN channel waveguides [64]. Once the NWs are deposited on the sample, their exact location can be referenced and SiN waveguides can be fabricated through dielectric deposition and e-beam lithography techniques. Fig. 17(b) shows SiN waveguide devices, incorporating ring resonator filters, coupled to NW sources.

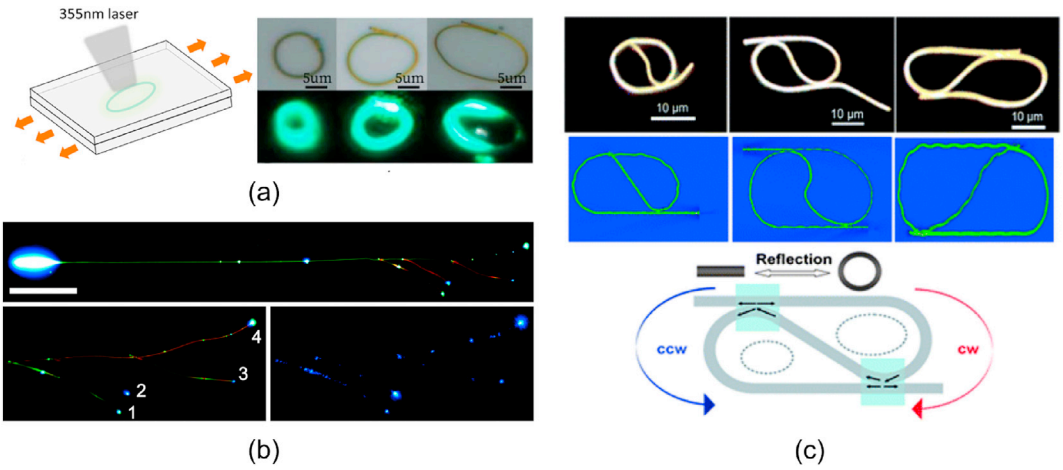

Fig. 16. (a) Self-coupled NW ring laser embedded in a polymer material as a strain sensor. Reprinted with permission from Ref. [62]. Copyright 2020 John Wiley & Sons, Inc. (b) Networks of NW devices integrated to allow evanescent field coupling between individual NWs, reprinted with permission from Ref. [38]. Copyright (2005) National Academy of Sciences, U.S.A. (c) Fabry-Perot NW lasers, formed into self-coupled feedback structures. (top) optical images (middle) numerical simulations of guided fields and (bottom) schematic. Republished with permission of Royal Society of Chemistry, from Ref. [61].

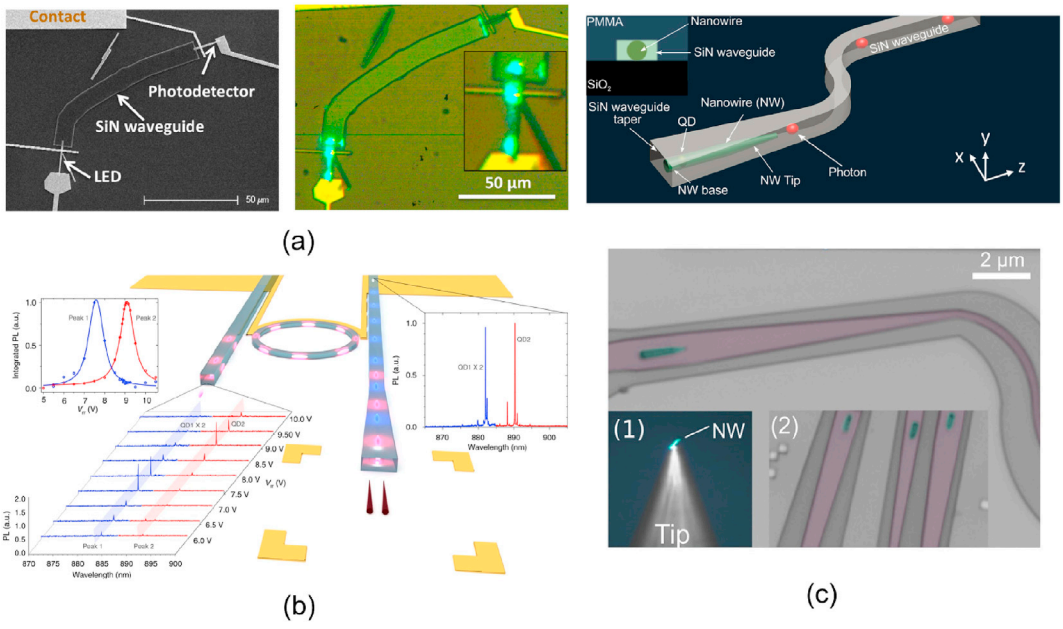

Fig. 17. (a) (left) SEM and (right) optical microscope images of a SiN channel waveguide post-fabricated between InGaN NW source and emitters with electronic contacts. Adapted with permission from Ref. [63]. Copyright 2014 American Chemical Society. (b) Schematic of two quantum dot containing tapered NWs coupled to the facet of a SiN waveguide. The SiN circuit incorporates a ring resonator filter and inset graphs show measured spectra from the NW emitters into the bus waveguide and the drop port of the ring, the latter as a function of bias voltage on the ring thermal tuning element. Adapted under CC-BY 4.0 license from Nature Communications 8 (2017). Copyright 2017 The Authors [27]. (c) Schematic and optical microscope images of a tapered semiconductor NW embedded in a SiN waveguide. Adapted with permission from Nano Letters 16, 5b04709 [64]. Copyright 2016 American Chemical Society.

3.4.3. Pre-NW-transfer waveguide fabrication

If the spatial accuracy of NW transfer to a receiver chip is good enough, devices can be integrated with pre-fabricated waveguide devices. This is a more attractive route for scaling as it does not require registration of NW position to inform waveguide fabrication, and is therefore compatible with the maturing availability of foundry-fabricated Photonic Integrated Circuits (PICs).

Direct coupling of NWs transferred at the end facets, or evanescently coupled to the top surface of waveguides and cavities [65], has been demonstrated. Waveguide platforms in SiN [14] and polymer-on-glass [49] have been coupled to semiconductor NW devices, as

shown in Fig. 18(a). In Ref. [14] the authors demonstrate direct alignment of a quantum dot emitter in a tapered NW, transferred onto a compact SiN waveguide. The high precision alignment achieved using in-situ SEM monitoring allows for high efficiency coupling between the NW and the waveguide, as shown in Fig. 3(b). In Ref. [49] the authors directly print individual NWs onto SU8 polymer waveguides, demonstrating multiple wavelength devices on a single waveguide, and operation of the full chip under mechanical deformation.

Bao et al. [30] present an integrated silicon nitride Mach-Zehnder Interferometer (MZI) device where one of the interferometer arms is formed using a heterogeneously integrated CdS NW. In this work the authors use pre-fabricated silicon nitride PIC devices as a receiver substrate and a micro-probe based NW manipulation method to accurately place the CdS NWs on the MZI, as shown in Fig. 18(b). Shearing of the NW against the silicon nitride waveguide coupler sections ensures effective optical coupling and accurate NW deposition on the receiver chip. By using the length of the coupler sections as a variable, the authors demonstrate control over the coupling efficiency between the on-chip waveguides and CdS NW devices.

Transfer of NW devices to sub-micron scale waveguide structures have been demonstrated using surface topology to ensure the necessary control on spatial alignment. As noted previously, NW laser devices have been integrated with plasmonic V-groove waveguides demonstrating direct coupling between NW and V-groove waveguide modes, and vertical emission from angled facet terminations [37]. Using a similar methodology Sergent et al. [28] demonstrate coupling of NW devices with on-chip photonic crystal PC cavities. The PC devices are fabricated using e-beam lithography and reactive ion etching into silicon nitride and suspension of this layer by chemically selective etching of the silicon substrate. The PC cavities are fabricated with a central defect line, and incorporate a shallow groove to assist trapping of the NW devices with diameters of only a few tens of nanometres. The coupled effect of the PC and the NW produces a resonant cavity in the NW, enhancing emission efficiency and with resonant wavelength set by the PC periodicity, as shown in Fig. 19.

4. Scaling

Many of the demonstrations of NW device integration presented in the previous sections are proof of concept devices incorporating a small number of NWs on-chip. In order to fully exploit the potential of NW devices as building block components in integrated optical, electronic and NEMS systems feasible routes towards scalable integration are being sought.

Before discussing the integration of NWs at scale, it is worth considering the complementary requirement of selecting single devices from large populations of NWs in their initial, randomly distributed state on an intermediate substrate. Without pre-characterising and spatially selecting devices, a degree of inhomogeneity in target device properties across a population can be expected [66]. One technique to deal with such inhomegeneity in single device characteristics can be to use a multiplexed integration method where individual NWs can be electronically addressed from a hierarchical structure [67]. This technique allows for detailed measurements of a set of devices on a single substrate, where selection between individual devices may be resource intensive, for example in-situ cryogenic measurements. Alternatively, nesting such architectures in a wider circuit design can mitigate for device to device variations.

Recent advances in high throughput, optical microscopy based characterisation allow multiple measurements to be carried out on a single system and can be combined with high-resolution translation stage control to provide spatial location information on the devices under test. Alanis et al. [68] demonstrate a single measurement system that first locates NW optical emitters in a wide field of view mode by fluorescence. Each emitter position is then registered relative to on-chip markers. In high magnification mode the system can select individual emitters in series, measuring pump energy dependent spectra, lasing threshold, bright and darkfield imaging to determine NW location and rotational orientation and even pump beam polarisation dependence of optical emission. Since this dataset is related to the spatial position and orientation of the NW devices, individual devices can be easily located for further processing.

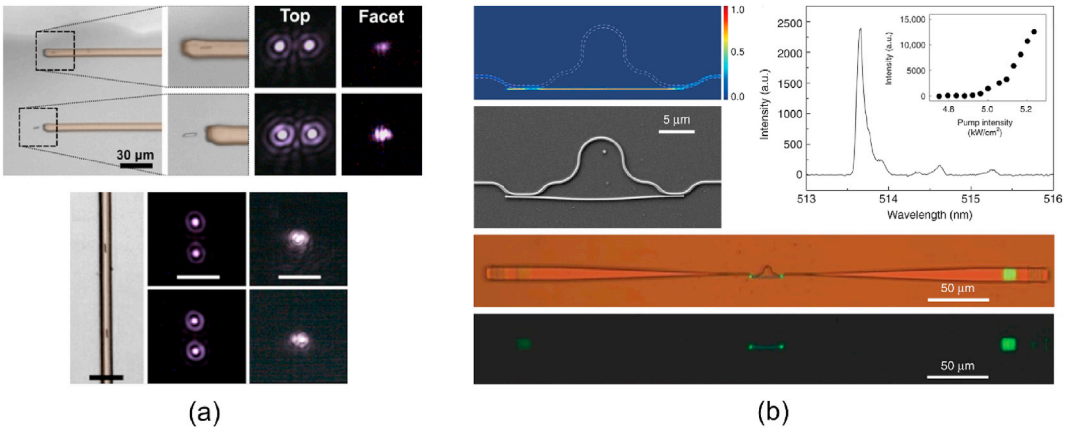

Fig. 18. (a) Optical microscope images showing NW lasers printed at the facets and on top of polymer waveguides. Dark field images show emission from the sample surface and waveguide facet. Adapted with permission from Ref. [49]. Copyright 2017 American Chemical Society. (b) SEM and optical microscope images of a CdS NW integrated directly in contact with a waveguide Mach-Zehnder interferometer.Inset shows lasing spectrum. Adapted under CC-BY 4.0 license from Light: Science & Applications 8 (2020). Copyright 2020 The Authors [30].

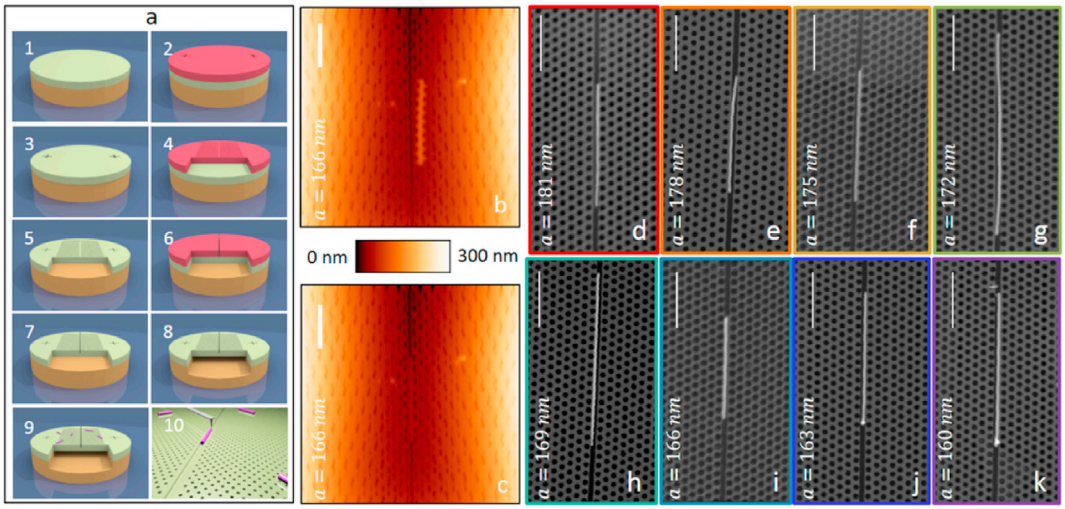

Fig. 19. Schematic fabrication process (left) AFM (centre) and SEM images (right) of NWs aligned with topological grooves in a SiN photonic crystal. Reprinted with permission from Ref. [28]. Copyright 2017 American Chemical Society.

In Ref. [69] Jevtics et al. make use of the high throughput microscopy system to select NW laser devices by threshold performance and transfer these to a secondary substrate. The spatial position of the NWs measured by the microscopy measurement system is then used as an input to the transfer printing instrument used for NW processing, see Fig. 20. The compatibility of the high-accuracy translation stages, optical microscopes and marker recognition on both systems allows for sub-micron automated alignment of the NW transfers.

NW transfer based processes are inherently serial due to the requirement of selecting single NWs from randomly distributed populations. An alternative method has been reported by which populations of NWs can be grown in site-specific locations on-chip and with a growth axis angled with respect to the sample plane, as compared with NWs typically grown vertically. Schvartzman et al. [70] present arrayed growth of NWs, where the angle made between the NW and the substrate, Fig. 21, allows groups of NWs to be cleaved and deposited onto the growth substrate, preserving the lithographic arrangement of devices and relative placement with respect to on-chip registration marks. Further lithographic processes are then carried out to define electronic contacts and tracks aligned with NW arrays, making this process compatible with common optoelectronic chipscale fabrication processes.

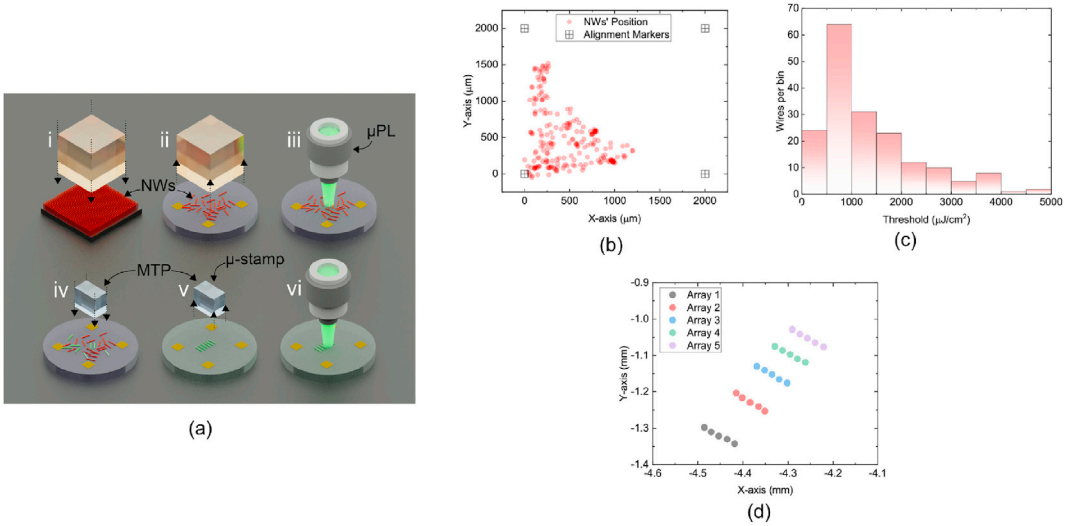

Fig. 20. (a) Schematic of device measurement, binning, and reprinting process. (b) Spatial map of population of NW laser devices. (c) Measured NW lasers binned by threshold energy. (d) Spatial map of selected NWs transfer printed onto a receiver substrate. Adapted with permission from Nano Letters 20, 9b05078 [69]. Copyright 2020 American Chemical Society.

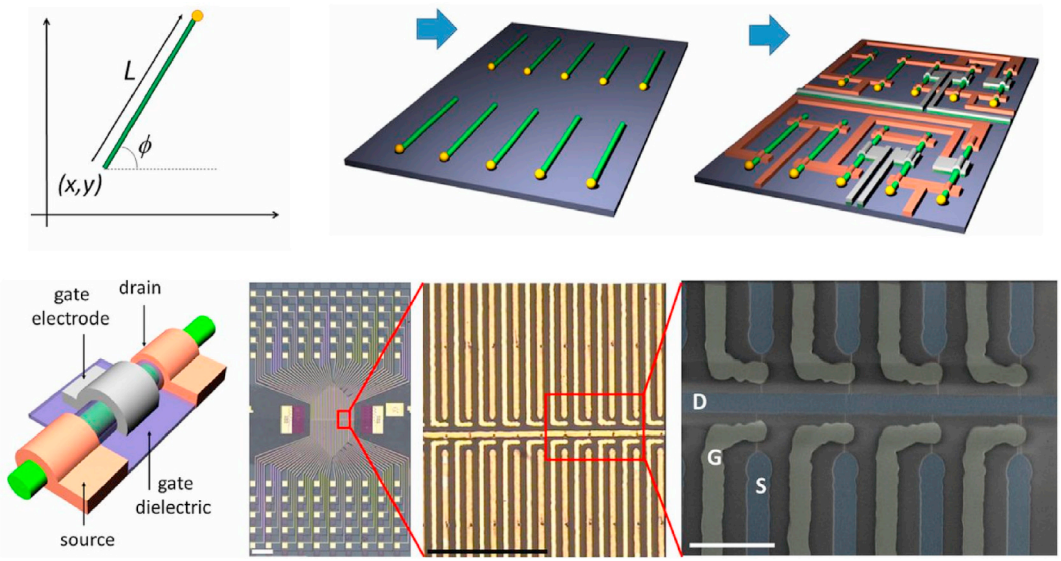

Fig. 21. Top row: scheme for selective directional growth of NW devices and integration with lithographically defined electronic contacts. Bottom row: micrographs of fabricated NW transistor devices. Reprinted with permission from Ref. [70].

5. Conclusion

As the growth and fabrication of NW devices matures it is clear that methods are required by which these compact devices can be deterministically integrated into chipscale photonic and electronic systems. Individual NWs have been integrated with on-chip elements including electronic contacts, surface gratings, waveguides and even other NW devices. The variety of transfer processes available allow for fabrication flows where NWs are deposited before further processing or with high spatial accuracy, post-fabrication of micron scale circuit elements. The complementarity of high throughput measurement and NW transfer processes provide early indications of potential routes to scaling of these processes, taking demonstrations from proof-of-concept experiments towards manufacturing compatible micro-assembly. Recent advances in site specific NW growth have shown compatibility with lithographic processing and scaling, and together with high accuracy transfer printing techniques, offer an attractive prospect for future multi-material, parallel integration of populations of NW devices at scale.

Acknowledgments

This work was supported in part by the Engineering and Physical Sciences Research Council (EP/P013597/1, EP/R03480X/1, EP/V004859/1, EP/V025198/1), the Royal Academy of Engineering under the Research Chairs and Senior Research fellowships scheme and the European Commission (Grant 828841-ChipAI-H2020-FETOPEN-2018-2020). We wish to thank Chennupati Jagadish and Hark Hoe Tan (ANU), Hannah Joyce (Cambridge), Michael Johnstone (Oxford) and Patrick Parkinson (Manchester) for their support of our work on NW transfer printing.

References

[1] Gregor Koblmüller, Benedikt Mayer, Thomas Stettner, Gerhard Abstreiter, Jonathan J. Finley, GaAs–AlGaAs core–shell nanowire lasers on silicon: invited review, Semicond. Sci. Technol. 32 (5) (May 2017), 053001.
[2] Michael H. Huang, Samuel Mao, Henning Feick, Haoquan Yan, Yiying Wu, Hannes Kind, Eicke Weber, Richard Russo, Peidong Yang, Room-temperature ultraviolet nanowire nanolasers, Science 292 (5523) (Jun 2001) 1897–1899.
[3] Qian Gao, Dhruv Saxena, Fan Wang, Lan Fu, Sudha Mokkapati, Yanan Guo, Li Li, Jennifer Wong-Leung, Philippe Caroff, Hark Hoe Tan, Chennupati Jagadish, Selective-area epitaxy of pure wurtzite InP nanowires: high quantum efficiency and room-temperature lasing, Nano Lett. 14 (9) (2014) 5206–5211.
[4] Hyunseok Kim, Wook Jae Lee, Alan C. Farrell, Akshay Balgarkashi, L. Diana, Huffaker, Telecom-wavelength bottom-up nanobeam lasers on silicon-on-insulator, Nano Lett. 17 (9) (2017) 5244–5250.
[5] Xin Yan, Wei Wei, Fengling Tang, Xi Wang, Luying Li, Xia Zhang, Xiaomin Ren, Low-threshold room-temperature AlGaAs/GaAs nanowire/single-quantum-well heterostructure laser, Appl. Phys. Lett. 110 (6) (Feb 2017), 061104.
[6] Silvija Gradečak, Fang Qian, Yat Li, Hong-Gyu Park, Charles M. Lieber, GaN nanowire lasers with low lasing thresholds, Appl. Phys. Lett. 87 (17) (Oct 2005) 173111.
[7] Qiming Li, Jeremy B. Wright, Weng W. Chow, Ting Shan Luk, Igal Brener, Luke F. Lester, George T. Wang, Single-mode GaN nanowire lasers, Opt Express 20 (16) (Jul 2012) 17873.
[8] Dhruv Saxena, Sudha Mokkapati, Patrick Parkinson, Nian Jiang, Qiang Gao, Hark Hoe Tan, Chennupati Jagadish, Optically pumped room-temperature GaAs nanowire lasers, Nat. Photonics 7 (12) (Dec 2013) 963–968.
[9] Shula Chen, Mattias Jansson, Jan E. Stehr, Yuqing Huang, Fumitaro Ishikawa, Weimin M. Chen, Irina A. Buyanova, Dilute nitride nanowire lasers based on a GaAs/GaNAs core/shell structure, Nano Lett. 17 (3) (Feb 2017) 1775–1781.

[10] Guoqiang Zhang, Masato Takiguchi, Kouta Tateno, Takehiko Tawara, Masaya Notomi, Hideki Gotoh, Telecom-band lasing in single InP/InAs heterostructure nanowires at room temperature, Sci. Adv. 5 (2) (Feb 2019).
[11] Dhruv Saxena, Nian Jiang, Xiaoming Yuan, Sudha Mokkapati, Yanan Guo, Hark Hoe Tan, Chennupati Jagadish, Design and room-temperature operation of GaAs/AlGaAs multiple quantum well nanowire lasers, Nano Lett. 16 (8) (Aug 2016) 5080–5086.
[12] Xin Li, Rong-Ling Su, Zhang-Kai Zhou, Ying Yu, Andrea Di Falco, Photonic trimming of quantum emitters via direct fabrication of metallic nanofeatures, APL Photonics 3 (7) (Jul 2018), 071301.
[13] Ritesh Agarwal, Kosta Ladavac, Yael Roichman, Guihua Yu, Charles M. Lieber, David G. Grier, Manipulation and assembly of nanowires with holographic optical traps, Opt Express 13 (22) (2005) 8906.
[14] Khaled Mnaymneh, Dan Dalacu, Joseph McKee, Jean Lapointe, Sofiane Haffouz, John F. Weber, David B. Northeast, Philip J. Poole, Geof C. Aers, Robin L. Williams, On-chip integration of single photon sources via evanescent coupling of tapered nanowires to SiN waveguides, Adv. Quant. Technol. 3 (2) (Feb 2020) 1900021.
[15] Guo-Wei Zha, Xiang-Jun Shang, Hai-Qiao Ni, Ying Yu, Jian-Xing Xu, Si-Hang Wei, Ben Ma, Li-Chun Zhang, Zhi-Chuan Niu, In situ probing and integration of single self-assembled quantum dots-in-nanowires for quantum photonics, Nanotechnology 26 (38) (Sep 2015) 385706.
[16] Yu Huang, Xiangfeng Duan, Charles M. Lieber, Nanowires for integrated multicolor nanophotonics, Small 1 (1) (2005) 142–147.
[17] Xi Liu, Yun-Ze Long, Lei Liao, Xiangfeng Duan, Zhiyong Fan, Large-scale integration of semiconductor nanowires for high-performance flexible electronics, ACS Nano 6 (3) (Mar 2012) 1888–1900.
[18] Pan Dong, Mengqi Fu, Xuezhe Yu, Xiaolei Wang, Lijun Zhu, Shuaihua Nie, Siliang Wang, Qing Chen, Peng Xiong, Stephan Von Molnár, et al., Controlled synthesis of phase-pure inas nanowires on si(111) by diminishing the diameter to 10 nm, Nano Lett. 14 (3) (Mar 2014) 1214–1220.
[19] Jianping Meng, Li Zhou, J.P. Meng, Z. Li, Schottky-contacted nanowire sensors, Adv. Mater. 32 (28) (Jul 2020) 2000130.
[20] Carlos García Núñez, Fengyuan Liu, William Taube Navaraj, Adamos Christou, Dhayalan Shakthivel, Ravinder Dahiya, Heterogeneous integration of contact-printed semiconductor nanowires for high-performance devices on large areas, Microsyst. Nanoeng. 4 (1) (Aug 2018) 1–15, 2018 4:1.
[21] Andrew Carlson, Audrey M. Bowen, Yonggang Huang, Ralph G. Nuzzo, John A. Rogers, Transfer printing techniques for materials assembly and micro/Nanodevice fabrication, Adv. Mater. 24 (39) (Oct 2012) 5284–5318.
[22] Juan Arturo Alanis, Qian Chen, Mykhaylo Lysevych, Tim Burgess, Li Li, Liu Zhu, Hark Hoe Tan, Chennupati Jagadish, Patrick Parkinson, Threshold reduction and yield improvement of semiconductor nanowire lasers via processing-related end-facet optimization, Nanoscale Adv. 1 (11) (2019) 4393–4397.
[23] H. Gao, A. Fu, S.C. Andrews, P. Yang, Cleaved-coupled nanowire lasers, Proc. Natl. Acad. Sci. 110 (3) (Jan 2013) 865–869.
[24] Hyunseok Kim, Wook-Jae Lee, Alan C. Farrell, Juan S.D. Morales, Pradeep Senanayake, Sergey V. Prikhodko, Tomasz J. Ochalski, Diana L. Huffaker, Monolithic InGaAs nanowire array lasers on silicon-on-insulator operating at room temperature, Nano Lett. 17 (6) (Jun 2017) 3465–3470.
[25] Chunhuan Zhang, Chang-ling Zou, Haiyun Dong, Yongli Yan, Jiannian Yao, Yong Sheng Zhao, Dual-color single-mode lasing in axially coupled organic nanowire resonators, Sci. Adv. 3 (7) (2017), e1700225.
[26] Jianwei Yan, Yang Chen, Xiaowu Wang, Ying Fu, Juxiang Wang, Sun Jia, Guozhang Dai, Shaohua Tao, Yongli Gao, High-performance solar-blind sno 2 nanowire photodetectors assembled using optical tweezers, Nanoscale 11 (2019).
[27] Ali W. Elshaari, Iman Esmaeil Zadeh, Andreas Fognini, Michael E. Reimer, Dan Dalacu, Philip J. Poole, Val Zwiller, Klaus D. Jöns, On-chip single photon filtering and multiplexing in hybrid quantum photonic circuits, Nat. Commun. 8 (1) (Dec 2017) 379.
[28] Sylvain Sergent, Masato Takiguchi, Tsuchizawa Tai, Atsushi Yokoo, Hideaki Taniyama, Eichi Kuramochi, Masaya Notomi, Nanomanipulating and tuning ultraviolet zno-nanowire-induced photonic crystal nanocavities, ACS Photonics 4 (5) (2017) 1040–1047.
[29] Xin Guo, Min Qiu, Jiming Bao, Benjamin J. Wiley, Qing Yang, Xining Zhang, Yaoguang Ma, Huakang Yu, Limin Tong, Direct coupling of plasmonic and photonic nanowires for hybrid nanophotonic components and circuits, Nano Lett. 9 (12) (Dec 2009) 4515–4519.
[30] Qingyang Bao, Weijia Li, Peizhen Xu, Ming Zhang, Daoxin Dai, Pan Wang, Xin Guo, Limin Tong, On-chip single-mode CdS nanowire laser, Light Sci. Appl. 9 (1) (Dec 2020) 42.
[31] Yao Xiao, Chao Meng, Pan Wang, Yu Ye, Huakang Yu, Shanshan Wang, Fuxing Gu, Lun Dai, Limin Tong, Single-nanowire single-mode laser, Nano Lett. 11 (3) (Mar 2011) 1122–1126.
[32] Atsushi Yokoo, Masato Takiguchi, Muhammad Danang Birowosuto, Kouta Tateno, Guoqiang Zhang, Eiichi Kuramochi, Akihiko Shinya, Hideaki Taniyama, Masaya Notomi, Subwavelength nanowire lasers on a silicon photonic crystal operating at telecom wavelengths, ACS Photonics 4 (2) (2017) 355–362.
[33] Masato Takiguchi, Atsushi Yokoo, Kengo Nozaki, Muhammad Danang Birowosuto, Kouta Tateno, Guoqiang Zhang, Eiichi Kuramochi, Akihiko Shinya, Masaya Notomi, Continuous-wave operation and 10-gb/s direct modulation of inasp/inp sub-wavelength nanowire laser on silicon photonic crystal, APL Photonics 2 (4) (2017), 046106.
[34] Edgars Butanovs, Jelena Butikova, Aleksejs Zolotarjovs, Boris Polyakov, Towards metal chalcogenide nanowire-based colour-sensitive photodetectors, Opt. Mater. 75 (Jan 2018) 501–507.
[35] Mei Liu, Djoulde Aristide, Quan Yang, Weilin Su, Lingli Kong, Jinjun Rao, Jinbo Chen, Zhiming Wang, Nanorobotic manipulation inside scanning electron microscope for the electrical and mechanical characterization of zno nanowires, in: Proceedings of the 16th Annual IEEE International Conference on Nano/Micro Engineered and Molecular Systems, NEMS 2021, Apr 2021, pp. 919–924.
[36] Huiwen Xu, Jeremy B. Wright, Luk Ting-shan, Jeffery J. Figiel, Karen Cross, Luke F. Lester, George T. Wang, Igal Brener, Qiming Li, Single-mode lasing of GaN nanowire-pairs, Appl. Phys. Lett. 113106 (2012) (2014) 8–12.
[37] Esteban Bermúdez-Ureña, Gozde Tutuncuoglu, Javier Cuerda, L. Cameron, C. Smith, Jorge Bravo-Abad, Sergey I. Bozhevolnyi, Anna Fontcuberta i Morral, Francisco J. García-Vidal, Romain Quidant, Plasmonic waveguide-integrated nanowire laser, Nano Lett. 17 (2) (Feb 2017) 747–754.
[38] Donald J. Sirbuly, Matt Law, Pauzauskie Peter, Haoquan Yan, Alex V. Maslov, Knutsen Kelly, Cun-Zheng Ning, Richard J. Saykally, Peidong Yang, Optical routing and sensing with nanowire assemblies, Proc. Natl. Acad. Sci. U.S.A. 102 (22) (2005) 7800–7805.
[39] Peter A. Smith, Christopher D. Nordquist, Thomas N. Jackson, Theresa S. Mayer, Benjamin R. Martin, Jeremiah Mbindyo, E. Thomas, Mallouk, Electric-field assisted assembly and alignment of metallic nanowires, Appl. Phys. Lett. 77 (9) (Aug 2000) 1399–1401.
[40] Mindaugas Gecevič Ius, Rokas Drevinskas, Martynas Beresna, Peter G. Kazansky, Single beam optical vortex tweezers with tunable orbital angular momentum, Appl. Phys. Lett. 104 (23) (2014) 15–19.
[41] Maria G. Donato, Oto Brzobohatý, Stephen H. Simpson, Alessia Irrera, Antonio A. Leonardi, J. Maria, Faro Lo, Vojtěch Svak, Onofrio M. Maragò, Pavel Zemánek, Optical trapping, optical binding, and rotational dynamics of silicon nanowires in counter-propagating beams, Nano Lett. 19 (1) (2019) 342–352.
[42] Peter J. Reece, Wen Jun Toe, Fan Wang, Suriati Paiman, Qiang Gao, H. Hoe Tan, C. Jagadish, Characterization of semiconductor nanowires using optical tweezers, Nano Lett. 11 (6) (Jun 2011) 2375–2381.
[43] Benoit Guilhabert, Antonio Hurtado, Dimitars Jevtics, Qian Gao, Hark Hoe Tan, Chennupati Jagadish, D. Martin, Dawson, Transfer printing of semiconductor nanowires with lasing emission for controllable nanophotonic device fabrication, ACS Nano 10 (4) (Apr 2016) 3951–3958.
[44] Brian Corbett, Ruggero Loi, Weidong Zhou, Liu Dong, Zhenqiang Ma, Transfer print techniques for heterogeneous integration of photonic components, Prog. Quant. Electron. 52 (1–17) (Mar 2017).
[45] A.J. Trindade, B. Guilhabert, D. Massoubre, D. Zhu, N. Laurand, E. Gu, I.M. Watson, C.J. Humphreys, M.D. Dawson, Nanoscale-accuracy transfer printing of ultra-thin AlInGaN light-emitting diodes onto mechanically flexible substrates, Appl. Phys. Lett. 103 (25) (2013) 253302.
[46] John McPhillimy, Benoit Guilhabert, Charalambos Klitis, Martin D. Dawson, Marc Sorel, Michael John Strain, High accuracy transfer printing of single-mode membrane silicon photonic devices, Opt Express 26 (13) (2018) 297–300.
[47] Dimitars Jevtics, Jack A. Smith, John McPhillimy, Benoit Guilhabert, Paul Hill, Charalambos Klitis, Antonio Hurtado, Marc Sorel, Hark Hoe Tan, Chennupati Jagadish, Martin D. Dawson, J. Michael, Strain. Spatially dense integration of micron-scale devices from multiple materials on a single chip via transfer-printing, Opt. Mater. Express 11 (10) (Oct 2021) 3567.
[48] John McPhillimy, Dimitars Jevtics, Benoit J.E. Guilhabert, Charalambos Klitis, Antonio Hurtado, Marc Sorel, Martin D. Dawson, Michael J. Strain, Automated nanoscale Absolute accuracy alignment system for transfer printing, ACS Appl. Nano Mater. 3 (10) (Oct 2020) 10326–10332.

[49] Dimitars Jevtics, Antonio Hurtado, Benoit Guilhabert, John McPhillimy, Giuseppe Cantarella, Qian Gao, Hark Hoe Tan, Chennupati Jagadish, Michael J. Strain, Martin D. Dawson, Integration of semiconductor nanowire lasers with polymeric waveguide devices on a mechanically flexible substrate, Nano Lett. 17 (10) (Oct 2017) 5990–5994.
[50] Wei-Zong Xu, Fang-Fang Ren, Dimitars Jevtics, Antonio Hurtado, Li Li, Qian Gao, Jiandong Ye, Fan Wang, Benoit Guilhabert, Lan Fu, Hai Lu, Rong Zhang, Hark Hoe Tan, Martin D. Dawson, Chennupati Jagadish, Vertically emitting indium phosphide nanowire lasers, Nano Lett. 18 (6) (Jun 2018) 3414–3420.
[51] Jeremy B. Wright, Salvatore Campione, Sheng Liu, Julio A. Martinez, Huiwen Xu, Ting S. Luk, Qiming Li, George T. Wang, Brian S. Swartzentruber, Luke F. Lester, Igal Brener, Distributed feedback gallium nitride nanowire lasers, Appl. Phys. Lett. 104 (4) (Jan 2014), 041107.
[52] Zongyin Yang, Tom Albrow-Owen, Hanxiao Cui, Jack Alexander-Webber, Fuxing Gu, Xiaomu Wang, Tien-Chun Wu, Minghua Zhuge, Calum Williams, Pan Wang, Anatoly V. Zayats, Weiwei Cai, Lun Dai, Stephan Hofmann, Mauro Overend, Limin Tong, Qing Yang, Zhipei Sun, Tawfique Hasan, Single-nanowire spectrometers, Science 365 (6457) (Sep 2019) 1017–1020.
[53] Wenjin Luo, Qianchun Weng, Mingsheng Long, Peng Wang, Fan Gong, Hehai Fang, Man Luo, Wenjuan Wang, Zhen Wang, Dingshan Zheng, et al., Room-temperature single-photon detector based on single nanowire, Nano Lett. 18 (9) (Sep 2018) 5439–5445.
[54] Yi Zhu, Vidur Raj, Ziyuan Li, Hark Hoe Tan, Chennupati Jagadish, Lan Fu, Self-powered inp nanowire photodetector for single-photon level detection at room temperature, Adv. Mater. (2021).
[55] Kun Peng, Dimitars Jevtics, Fanlu Zhang, Sabrina Sterzl, Djamshid A. Damry, Mathias U. Rothmann, Benoit Guilhabert, Michael J. Strain, Hark H. Tan, Laura M. Herz, Lan Fu, Martin D. Dawson, Antonio Hurtado, Chennupati Jagadish, B. Michael, Johnston, Three-dimensional cross-nanowire networks recover full terahertz state, Science 368 (6490) (May 2020) 510–513.
[56] Yunyan Zhang, Dhruv Saxena, Aagesen Martin, Huiyun Liu, Toward electrically driven semiconductor nanowire lasers, Nanotechnology 30 (19) (2019).
[57] Masato Takiguchi, Guoqiang Zhang, Satoshi Sasaki, Kengo Nozaki, Edward Chen, Kouta Tateno, Takehiko Tawara, Akihiko Shinya, Hideki Gotoh, Masaya Notomi, Direct modulation of a single InP/InAs nanowire light-emitting diode, Appl. Phys. Lett. 112 (25) (June 2018) 251106.
[58] Xiangfeng Duan, Yu Huang, Ritesh Agarwal, Charles M. Lieber, Single-nanowire electrically driven lasers, Nature 421 (6920) (Jan 2003) 241–245.
[59] Wataru Tomita, Satoshi Sasaki, Kouta Tateno, Hajime Okamoto, Hiroshi Yamaguchi, Novel fabrication technique of suspended nanowire devices for nanomechanical applications, Phys. Status Solidi (b) 257 (2) (Feb 2020) 1900401.
[60] Maximilian Zapf, Robert Röder, Karl Winkler, Lisa Kaden, Johannes Greil, Marcel Wille, Marius Grundmann, Rüdiger Schmidt-Grund, Alois Lugstein, Carsten Ronning, Dynamical tuning of nanowire lasing spectra, Nano Lett. 17 (11) (2017) 6637–6643.
[61] Hanyang Li, Li Jin, Liangsheng Qiang, Yundong Zhang, Hao Sue, Single-mode lasing of nanowire self-coupled resonator, Nanoscale 5 (14) (Jun 2013) 6297–6302.
[62] Shengkun Li, Xin Li, Qin Yue, Yuejin Zhao, Local strain gauge based on the nanowires ring resonator embedded in a flexible substrate, Micro & Nano Lett. 15 (14) (Dec 2020) 1028–1032.
[63] M. Tchernycheva, A. Messanvi, A. De Luna Bugallo, G. Jacopin, P. Lavenus, L. Rigutti, H. Zhang, Y. Halioua, F.H. Julien, J. Eymery, et al., Integrated photonic platform based on InGaN/GaN nanowire emitters and detectors, Nano Lett. 14 (6) (Jun 2014) 3515–3520.
[64] Iman Esmaeil Zadeh, Ali W. Elshaari, Klaus D. Jöns, Andreas Fognini, Dan Dalacu, Philip J. Poole, Michael E. Reimer, Val Zwiller, Deterministic integration of single photon sources in silicon based photonic circuits, Nano Lett. 16 (4) (Apr 2016) 2289–2294.
[65] Linpeng Gu, Liang Fang, Qingchen Yuan, Xuetao Gan, Hao Yang, Xutao Zhang, Juntao Li, Hanlin Fang, Vladislav Khayrudinov, Harri Lipsanen, Zhipei Sun, Jianlin Zhao, Nanowire-assisted microcavity in a photonic crystal waveguide and the enabled high-efficiency optical frequency conversions, Photon. Res. 8 (11) (Nov 2020) 1734.
[66] Aaron Z. Goldberg, Andrei B. Klimov, al Gerd Leuchs, Ruqaiya Al-Abri, Hoyeon Choi, Patrick Parkinson, Measuring, controlling and exploiting heterogeneity in optoelectronic nanowires, J. Phys.: Photonics 3 (2) (Feb 2021), 022004.
[67] Luke W. Smith, Jack O. Batey, Jack A. Alexander-Webber, Ye Fan, Yu-Chiang Hsieh, Shin-Jr Fung, Dimitars Jevtics, Joshua Robertson, J. Benoit, E. Guilhabert, Michael J. Strain, Martin D. Dawson, Antonio Hurtado, Jonathan P. Griffiths, Harvey E. Beere, Chennupati Jagadish, Oliver J. Burton, Stephan Hofmann, Tse-Ming Chen, David A. Ritchie, Michael Kelly, Hannah J. Joyce, Charles G. Smith, High-throughput electrical characterization of nanomaterials from room to cryogenic temperatures, ACS Nano 14 (11) (Nov 2020) 15293–15305.
[68] Juan Arturo Alanis, Dhruv Saxena, Sudha Mokkapati, Nian Jiang, Kun Peng, Xiaoyan Tang, Lan Fu, Hark Hoe Tan, Chennupati Jagadish, Patrick Parkinson, Large-scale statistics for threshold optimization of optically pumped nanowire lasers, Nano Lett. 17 (8) (Aug 2017) 4860–4865.
[69] Dimitars Jevtics, John McPhillimy, Benoit Guilhabert, Juan A. Alanis, Hark Hoe Tan, Chennupati Jagadish, Martin D. Dawson, Antonio Hurtado, Patrick Parkinson, J. Michael, Strain. Characterization, selection, and microassembly of nanowire laser systems, Nano Lett. 20 (3) (Mar 2020) 1862–1868.
[70] M. Schvartzman, D. Tsivion, D. Mahalu, O. Raslin, E. Joselevich, Self-integration of nanowires into circuits via guided growth, Proc. Natl. Acad. Sci. 110 (38) (Sep 2013) 15195–15200.